Transient One Dimensional Numerical Simulation of Magnetoplasmadynamic Thrusters

by

Eliahu Haym Niewood

S.B. Aeronautics and Astronautics, Massachusetts Institute of Technology, 1987

SUBMITTED IN PARTIAL FULFILLMENT OF THE
REQUIREMENTS FOR THE DEGREE OF

Master of Science

in

Aeronautics and Astronautics

at the

Massachusetts Institute of Technology

Feb 1989

Signature of Author _____

Department of Aeronautics and Astronautics
Feb. 1989

Certified by _____

Professor Manuel Martinez-Sanchez, Thesis Supervisor
Department of Aeronautics and Astronautics

Accepted by _____

Professor Harold Y. Wachman, Chairman
Department Graduate Committee

Transient One Dimensional Numerical Simulation of Magnetoplasmadynamic Thrusters

by

Eliahu Haym Niewood

Submitted to the Department of
Aeronautics and Astronautics
in partial fulfillment of the
requirements for the degree of
Master of Science in Aeronautics and Astronautics

Magnetoplasmadynamic, or MPD, thrusters are a promising method of propulsion for a variety of different space missions. This research develops and analyzes a numerical simulation of a quasi one dimensional model for an MPD thruster. A finite difference scheme is used to integrate the fluid equations for each species and a magnetic field equation derived from Maxwell's laws. The model includes separate electron and heavy species temperatures, varying conductivity, varying ionization fraction, collisional energy transfer between heavy particles and electrons, averaged viscosity and ambipolar diffusion, and electron heat conduction. Both constant area and variable area channels are examined. The applied current in the cases studied ranges from 79.6 $\frac{kAmp}{meter\ depth}$ to 159$\frac{kAmp}{meter\ depth}$ for an inlet mass flow of 0.5 $\frac{kg}{m^2 \cdot sec}$. The length of the thruster is 0.2 meters with a minimum interelectrode separation of 0.02 meters. It is shown that thermal equilibrium is not a valid assumption in a typical MPD thruster. It is also found that viscosity plays a significant role in determining thruster performance. Area variation is also found to have a significant effect on performance.

Acknowledgements

I owe much gratitude to many people. I want to thank my advisor, Prof. Manuel Martinez-Sanchez, who has always been available when I needed advice and guidance. He has shown much patience with my mistakes, whether computer errors or misspellings. I would also like to thank the graduate students with whom I work, who have provided both technical help and friendship. They have made coming to work everyday almost enjoyable. I would particularly like to thank Eric Sheppard, for his help with MPD and his taking the time to edit my thesis, and Rodger Biasca, for his help with numerical methods, fluids, computers, and Latex. On a more personal note, I would like to thank Joanne for all her encouragement and understanding. Finally, I would like to thank my parents, who have done so much for me for so long.

This material is based upon work supported under a National Science Foundation Graduate Fellowship.

Contents

List of Figures

List of Tables

List of Symbols

$\vec{a}$ A vector quantity

$\hat{a}$ A unit vector in the a direction

a_{ref} Reference variable a

a_t Derivative of a with respect to time

a_z Derivative of a with respect to z position

a_{zz} Second derivative of a with respect to z position

$< a >$ Average of the quantity a

A Channel Area

a Speed of sound

α Ionization fraction

B Magnetic field strength

B_0 Inlet magnetic field strength

c_s Random velocity of species s

$\overline{C}_s$ Average thermal velocity of species s

d Channel width

D_a Ambipolar diffusion coefficient

Δt Time step

Δz Space step

E Electric field strength

E_l Elastic momentum transfer between electrons and heavy species

E_i Ionization energy

e Electric charge of a proton

ϵ_o Permittivity of vacuum

f_s Probability distribution of species s

F_s Force on species s

g Local convected flux

γ Ratio of specific heats

Γ_s Spitzer logarithm for species s

H Channel height

h Enthalpy

h_{t0} Inlet total enthalphy

I Total electric current

J Electric current density

k Boltzmann's constant

k_s Heat flux of species s

K_e Heat conduction coefficient

L Channel length

m_s mass of an atom of species s

μ Viscosity coefficient

μ_i Viscosity coefficient of ions

μ_n Viscosity coefficient of neutrals

μ_0 Permeability of vacuum

n_s Number density of species s

$\dot{n}_e$ Ionization rate

ν_{sr} Collision frequency of species s with species r

P_s Scalar fluid pressure of species s

P^* Sum of fluid and magnetic pressure

P Scalar fluid pressure

$\overline{\overline{P}}_s$ Pressure dyad

q_s Electric charge of a particle of species s

Q_{sr} Collision cross section of species s with species r

R_{mag} Magnetic Reynolds number

ρ_s Mass density of species s

$S1_s$ Source term for continuity equation of species s

$S2_s$ Source term for momentum equation of species s

$S3_s$ Source term for energy equation of species s

σ Scalar electrical conductivity

t Time

T_s Temperature of species s

U Average velocity of fluid

U_s Average velocity of species s

V Vector of integration variables

v_s Slip velocity of species s

w Velocity coordinate in phase space

Chapter 1

Introduction

In a conventional chemical thruster , the exit velocity of the gas is limited by the chemical energy contained in the propellants. Electric propulsion devices use electric power to add energy to the propulsive fluid, accelerating the fluid to velocities greater than those obtainable by standard chemical propulsion. Because a rocket's thrust is determined by the product of its mass flow and the gas exit velocity, electric propulsion devices produce more thrust than chemical rockets for the same fuel mass flow. However, electric propulsion requires power generating systems, which greatly increase system weight so that electric propulsion is a viable alternative to chemical propulsion in missions where the weight of the power generating system is less than the weight of the fuel saved.

A variety of different types of electric propulsion have been put forward as appropriate for space applications. One class of electric propulsion device is the magnetoplasmadynamic, or MPD thruster, which utilizes the Lorentz force produced by charged particles moving in a magnetic field to accelerate the propulsive fluid. An electric field is applied between electrodes as shown in Figure 1. The electrons in the plasma flow along the electric field lines, creating a current. The movement of the charged particles also creates a magnetic field, the "self-field", and in some devices an additional magnetic field is applied externally. A current in a magnetic field produces the Lorentz force, which accelerates the plasma in the axial direction, producing thrust. Gasdynamic forces also produce some thrust, but it is usually much smaller than the electromagnetic thrust.

MPD channels, because of the interaction between the magnetic field and the fluid, are extremely complicated and hard to analyze. One possible way to understand these devices, and to predict their performance, is to simulate them numerically. Numerical models have been used successfully in analyzing fluid flows in the absence of electric and magnetic fields. Some numerical work has been done with MPD thrusters. A number of works deal with steady quasi one dimensional flow. Martinez [10] and Kuriki [8] study a one fluid, fully ionized model. Minakuchi [13] includes the effect of heat conduction.

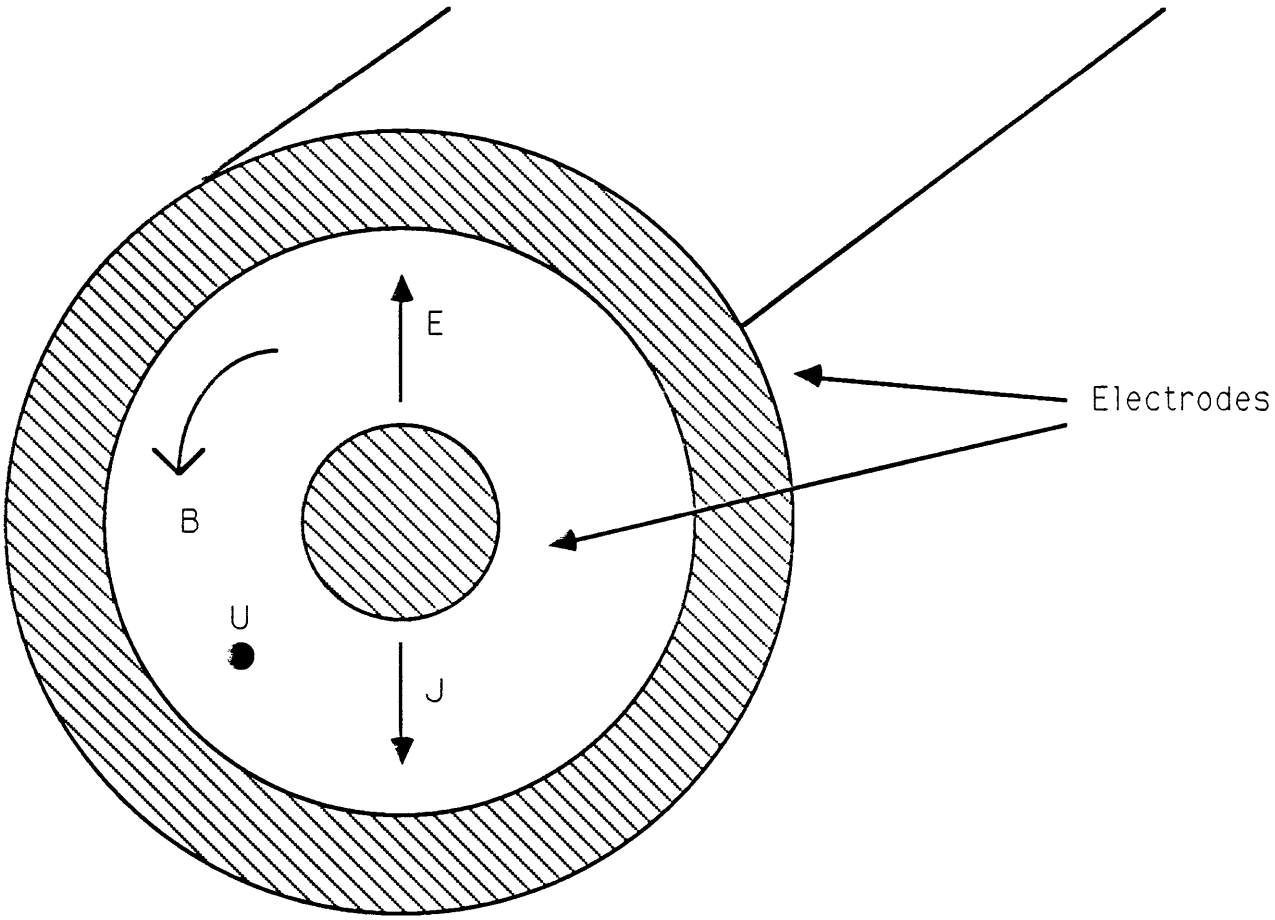

Figure 1.1: A MPD Thruster

Subramaniam [19] and Lawless [9] worked with both the one fluid model and a partly ionized two fluid model with thermal equilibrium. They include both viscosity and heat conduction to the wall in their model. Heimerdinger [3] also works with a partly ionized, thermal equilibrium model, which includes viscosity. Other existing works, by Chanty [2], Sleziona [18], and Park [14] examine fully two dimensional flow in both steady and unsteady cases, again with a one fluid, fully ionized model.

This research examines transient quasi one dimensional flow, using a two fluid model. Unlike previous research, the model allows for different heavy particle and electron temperatures, although it assumes that all species have the same average axial velocity. Viscosity and ambipolar diffusion across the channel, axial heat conduction, and varying magnetic conductivity are all included in the model. Although only steady state results are presented herein, the numerical methods used are equally applicable to transient flow. The model is discussed in detail in Chapter 2. The numerical methods used to perform

the simulation are detailed in Chapter 3. Chapter 4 gives the results of this method for a one fluid model similar to Martinez[10]. Chapters 5 and 6 describe the two fluid results for a constant area channel. Chapter 7 details results for a variable area channel.

There were a number of goals to this research. The first was simply to develop a numerical method with which to analyze an unsteady two fluid model of an MPD thruster. A second goal was to determine the effects of viscosity on thruster performance and gas temperature. The third goal was to find an ionization instability as the fluid neared full ionization. Finally, it was desired to determine the effects of area variation.

Chapter 2

Model and Equations

Self field MPD thrusters involve the highly complex interaction of ions, electrons, and neutrals in the working fluid with their induced magnetic field. The equations which govern this interaction are Maxwell's equations, Ohm's Law, and fluid equations.

2.1 Maxwell's Equations and Ohm's Law

In vector form, Maxwell's Equations are

$$\nabla \times \vec{B} = \frac{1}{\mu_0}(\vec{J} + \varepsilon_0 \frac{\partial \vec{E}}{\partial t}) \tag{2.1}$$

$$\nabla \times \vec{E} = -\frac{\partial \vec{B}}{\partial t} \tag{2.2}$$

$$\nabla \cdot \vec{B} = 0 \tag{2.3}$$

$$\nabla \cdot \vec{E} = \frac{e(n_i - n_e)}{\varepsilon_0} \tag{2.4}$$

The generalized Ohm's Law is

$$\vec{J} = \sigma(\vec{E} + \vec{U} \times \vec{B}) - (\frac{\sigma}{n_e e}\vec{J} \times \vec{B}) \tag{2.5}$$

Note that these equations are given in MKS units. Unless stated otherwise, all quantities in this thesis are given in MKS units.

2.2 Fluid Equations

2.2.1 Generalized Moment Equation

The fluid equations can be obtained by taking moments of Boltzmann's equation

$$\frac{\partial f_s}{\partial t} + \vec{w} \cdot \nabla f_s + \frac{\vec{F}_s}{m_s} \cdot \nabla_w f_s = (\frac{\partial f_s}{\partial t})_{collision} \tag{2.6}$$

where the generalized moment equation is found by integrating over velocity space the product of some function ϕ with the Boltzmann equation. The generalized moment equation is

$$\frac{\partial n_s < \phi >_s}{\partial t} - n_s < \frac{\partial \phi}{\partial t} > + \nabla \cdot (n_s < \phi_s \vec{w} >) - n_s < \vec{w} \cdot \nabla \phi >_s$$
$$-n_s < \frac{\vec{F}_s}{m_s} \cdot \nabla_w \phi >= \int_w (\frac{\partial f_s}{\partial t})_{collision} d^3 w \tag{2.7}$$

2.2.2 Mass Conservation

By taking $\phi = 1$ the species continuity equation is obtained

$$\frac{\partial \rho_s}{\partial t} + \nabla \cdot (\rho_s \vec{U}_s) = S1_s \tag{2.8}$$

where $S1_s$ represents a source term, $\rho_s = m_s n_s$, and $\vec{U}_s =< \vec{w} >_s$. By summing over all the species, electrons, ions, and neutrals, the overall mass conservation is obtained,

$$\frac{\partial \rho}{\partial t} + \nabla \cdot (\rho \vec{U}) = 0 \tag{2.9}$$

where $\rho = \sum_s \rho_s = m_i n_i + m_e n_e + m_n n_n \approx m_i n_i + m_n n_n$ and $\vec{U} = \frac{\sum_s (\rho_s U_s)}{\sum_s \rho_s}$

2.2.3 Momentum Conservation

The momentum equation can be found by taking the moment of Boltzmann's equation with $\phi = m_s \vec{w}$. The species momentum equation is then

$$\frac{\partial \rho_s \vec{U}_s}{\partial t} + \nabla \cdot (\rho_s \vec{U}_s \vec{U}_s + \overline{\overline{P}}'_s) = n_s q_s (\vec{E} + \vec{U}_s \times \vec{B}) + S2_s \tag{2.10}$$

where, $\overline{\overline{P}}'_s = \rho_s < \vec{c}_s \vec{c}_s >$. Again, by summing over all species, the overall momentum equation is found to be

$$\frac{\partial \rho \vec{U}}{\partial t} + \nabla \cdot (\rho \vec{U} \vec{U} + \overline{\overline{P}}) = \vec{J} \times \vec{B} + S2 \tag{2.11}$$

where, $\vec{v}_s$, the species slip velocity, is defined as $\vec{v}_s = \vec{U}_s - \vec{U}$, $\overline{\overline{P}}_s = \overline{\overline{P}}'_s + \rho_s \vec{v}_s \vec{v}_s$, and $\overline{\overline{P}} = \sum_s \overline{\overline{P}}_s$.

2.2.4 Energy Conservation

Choosing $\phi = \frac{1}{2} m_s (\vec{w} - \vec{U}_s)^2$ yields the species internal energy equation,

$$\frac{\partial (\frac{3}{2} \rho_s k T_s)}{\partial t} + \nabla \cdot (\frac{3}{2} \rho_s k T_s \vec{v}_s + \vec{k}_s) + \overline{\overline{P}}_s : \nabla \vec{U}_s = S3_s \tag{2.12}$$

where the state equation gives,

$$P_s = n_s k T_s \tag{2.13}$$

and $P_s = \frac{1}{3} Trace(\overline{\overline{P}}_s)$.

2.3 Model

The moment equations described earlier are only the first, second, and third moments of Boltzmann's equation. It is possible to take an infinite number of moments of this equation. However, by assuming relationships between $\overline{P}_s$ and $\overline{\overline{P}}_s$ and the other fluid variables, relationships given by the state equation 2.13, a closed set of equations is obtained using only the first three moments. For the purposes of this study, a number of additional simplifying assumptions are made. The first assumption is of quasi one dimensional flow. It is assumed that there are no variations in the y direction, and the variables in the fluid equations are assumed to be the average values across the channel in the x direction. Therefore, for the flow variables it is assumed that

$$\frac{\partial}{\partial x} = \frac{\partial}{\partial y} = 0 \tag{2.14}$$

Also there is only one component to the electric field, magnetic field and current, so that

$$\vec{B} = B\hat{y} \tag{2.15}$$

$$\vec{E} = E\hat{x} \tag{2.16}$$

$$\vec{J} = J\hat{x} \tag{2.17}$$

as shown in Figure 2.1. The model used herein is a two fluid model, so that the fluid is partially ionized and separate equations are needed for the electron and heavy particle temperature. However, it is assumed that all the particles have the same average velocity in the axial direction, so that

$$U_e = U_i = U_n = U \tag{2.18}$$

Also, the plasma is assumed to be neutral with singly ionized ions, so that

$$n_e = n_i \tag{2.19}$$

A one fluid model, used to test the algorithm, is discussed later in Section 2.9.

The working fluid in this model is Argon, with a molecular mass of $6.525 \times 10^{-26} \frac{kg}{particle}$ and an ionization energy of $2.53 \times 10^{-18} \frac{Joules}{particle}$.

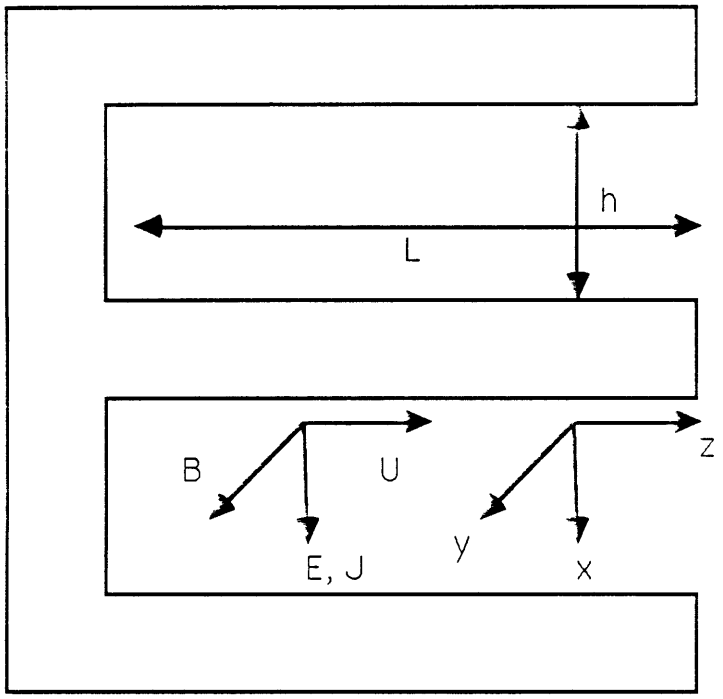

Figure 2.1: Quasi One Dimensional Model

2.3.1 Maxwell's Equations and Ohm's Law

In one dimensional form, Maxwell's equations, 2.1 - 2.4, become

$$\frac{\partial B}{\partial t} = -\frac{\partial E}{\partial z} \tag{2.20}$$

$$J = -\frac{1}{\mu_0}\frac{\partial B}{\partial z} \tag{2.21}$$

and Ohm's law, equation 2.5, is reduced to

$$E = \frac{J}{\sigma} + UB \tag{2.22}$$

where, assuming Coulomb collisions are dominant, σ is given by the Spitzer-Harm formula, $\sigma = \frac{0.0153 T_e^{\frac{3}{2}}}{\ln \Gamma_e}$ in Si, and $\Gamma_e = 1.24 \times 10^7 \sqrt{\frac{T_e^3}{n_e}}$

2.3.2 Magnetic Field Equation

By substituting equation 2.21 into Ohm's Law, equation 2.22, one obtains

$$E = \frac{1}{\sigma\mu_0}\frac{\partial B}{\partial z} + UB \tag{2.23}$$

Combining with equation 2.20

$$\frac{\partial B}{\partial t} + \frac{\partial UB}{\partial z} + \frac{1}{\sigma^2 \mu_0} \frac{\partial \sigma}{\partial z} \frac{\partial B}{\partial z} = \frac{1}{\sigma \mu_0} \frac{\partial^2 B}{\partial z^2} \tag{2.24}$$

2.3.3 Fluid Equations

The number of fluid equations which are necessary is determined by the number of unknown variables. Because all the types of heavy particles are assumed to have the same mean velocity, only one heavy particle momentum equation is needed, so only the overall momentum equation is used. Also, since the number of ions equals the number of electrons, only one species conservation equation is needed. In one dimension, the neccessary fluid equations 2.8 - 2.12 become

$$\frac{\partial \rho}{\partial t} + \frac{\partial \rho U}{\partial z} = 0 \tag{2.25}$$

$$\frac{\partial \rho U}{\partial t} + \frac{\partial (\rho U^2 + P + \frac{B^2}{2\mu_0})}{\partial z} = S2 \tag{2.26}$$

$$\frac{\partial \rho \alpha}{\partial t} + \frac{\partial \rho \alpha U}{\partial z} = m_i S1 \tag{2.27}$$

$$\frac{\partial \rho \alpha T_e}{\partial t} + \frac{\partial \rho \alpha U T_e}{\partial z} + \frac{2}{3} \rho \alpha T_e \frac{\partial U}{\partial z} = \frac{2}{3} \frac{m_i}{k} S3_e \tag{2.28}$$

$$\frac{\partial \rho T_g}{\partial t} + \frac{\partial \rho U T_g}{\partial z} + \frac{2}{3} \rho T_g \frac{\partial U}{\partial z} = \frac{2}{3} \frac{m_i}{k} S3_g \tag{2.29}$$

where $\alpha = \frac{n_e}{n_e + n_n}$.

2.4 Source Terms

The source terms in the electron density equation represent loss and creation of electrons. One process which contributes to this source term, is the rate of ionization due to electron impact, denoted by $\dot{n}_e$. This process is evaluated using the Hinnov-Hirshberg model of ionization [11], which gives

$$\dot{n}_e = R n_e [S n_n - n_e^2] \tag{2.30}$$

where,

$$R = \frac{1.09 \times 10^{-20}}{T_e^{\frac{9}{2}}} \; (in \; \frac{m^6}{sec}) \tag{2.31}$$

and

$$S = 2.9 \times 10^{22} T_e^{\frac{3}{2}} e^{-\frac{eV_i}{T_e}} \; (in \, m^{-3}) \tag{2.32}$$

Another process which contributes to the loss of electrons is loss to the walls due to ambipolar diffusion. Assuming a parabolic distribution for n_e,

$$n_e(x,z) = \frac{3}{2} n_e(z)[1 - (\frac{2x}{H})^2] \tag{2.33}$$

then

$$\frac{\partial^2 n_e}{\partial x^2} = \frac{12 n_e}{H^2} \tag{2.34}$$

where $n_e(z)$ is the average number density across the channel. So, the ambipolar diffusion is given by

$$\frac{\partial n_e}{\partial t} = D_a \frac{\partial^2 n_e}{\partial x^2} = \frac{12 D_a n_e}{H^2} \tag{2.35}$$

where D_a is the ambipolar diffusivity,

$$D_a = \sqrt{\frac{\pi k T_g}{4 m_i}} (1 + \frac{T_e}{T_g}) \frac{1}{Q_{in}(n_n + n_e)} \tag{2.36}$$

Combining both terms yields,

$$S1 = \dot{n}_e - \frac{12 D_a n_e}{H^2} \tag{2.37}$$

The source term in the momentum equation comes from the viscous forces exerted on the moving fluid by the walls, so that

$$S2 = -\frac{2\mu}{H} \left(\frac{\partial U}{\partial x} \right)_w \tag{2.38}$$

where μ, the coefficient of viscosity is given by [12],

$$\mu = \mu_n \frac{1-\alpha}{1 - \alpha + \alpha \frac{Q_{in}}{Q_{nn}}} + \mu_i \frac{\alpha}{(1-\alpha)\frac{Q_{in}}{Q_{ii}} + \alpha} \qquad (in \ \frac{kg}{m \cdot sec}) \tag{2.39}$$

$$\mu_n = \frac{m_i \overline{C}_i}{2 Q_{nn}} \qquad (in \ \frac{kg}{m \cdot sec})$$

$$\mu_i = \frac{0.406 (4\pi\epsilon_0)^2 \sqrt{m_i} (k T_g)^{\frac{5}{2}}}{e^4 \ln \Gamma_g} \qquad (in \ \frac{kg}{m \cdot sec})$$

$$Q_{nn} = 1.7 \times 10^{-18} T_g^{-\frac{1}{4}} \qquad (in \ m^2)$$

$$Q_{in} = 1.4 \times 10^{-18} \qquad (in \ m^2)$$

$$Q_{ii} = \frac{e^4 \ln \Gamma_g}{32 \pi \epsilon_o^2 k^2 T_g^2} \qquad (in \ m^2)$$

$$\overline{C}_i = \sqrt{\frac{8 k T_g}{\pi m_i}} \qquad (in \ \frac{m}{s})$$

$$\Gamma_g = 1.24 \times 10^7 \sqrt{\frac{T_g^3}{n_e}}$$

Again, a parabolic distribution is assumed for the velocity across the channel,

$$U(x,z) = \frac{3}{2}U(z)[1 - (\frac{2x}{H})^2] \tag{2.40}$$

and $\frac{\partial U}{\partial x}$ is evaluated at the wall to give

$$S2 = -\frac{12U\mu}{H^2} \tag{2.41}$$

The source term in the electron temperature equation represents ways in which energy can be taken from or absorbed by the electrons. One source of enery loss is the Joule heating, given by $\frac{J^2}{\sigma}$. Another source of energy is collisional energy transfer between electrons and the heavy particles, denoted by E_l, where

$$E_l = 5.67 \times 10^{-28}(T_e - Tg)n_e\nu_{ei} \qquad (in\ \frac{watts}{m^3}) \tag{2.42}$$

where,

$$\nu_{ei} = \frac{\overline{C}_e n_e Q_{ei}}{1.98} \qquad (in\ \frac{1}{s})$$

$$Q_{ei} = \frac{5.85 \times 10^{-10} ln\Gamma_e}{T_e^2} \qquad (in\ m^2)$$

$$\overline{C}_e = 6214.0\sqrt{T_e} \qquad (in\ \frac{m}{sec})$$

Since the internal energy as defined does not include the ionization energy of the electrons, energy is also lost when an electron ionizes, so there is a loss equal to $E_i\dot{n}_e$. Also included in this source term is the heat conduction, given by $\frac{\partial}{\partial z}(K_e\frac{\partial T_e}{\partial z})$, where [11],

$$K_e = \frac{1.7142k^2T_e\sigma}{e^2} \qquad (in\frac{watt}{m \cdot K}) \tag{2.43}$$

Including all of these processes,

$$S3_e = \frac{J^2}{\sigma} - E_l - E_i\dot{n}_e + \frac{\partial}{\partial z}(K_e\frac{\partial T_e}{\partial z}) \tag{2.44}$$

The source term for the heavy particle temperature equation includes the momentum lost to the electrons, described earlier, and the heat produced by the viscous force applied by the wall to the fluid. This heat is given by $\mu(\frac{\partial U}{\partial x})^2$, which is averaged over the channel assuming the parabolic velocity distribution given in equation 2.40 .

$$S3_g = E_l + \frac{12U^2\mu}{H^2} \tag{2.45}$$

2.5 Area Variation

The equations developed above are for a constant area channel. For a channel with varying area, where $A = HD = H\cdot$ (unit depth), the equations must be modified slightly. The set of modified equations are

$$\frac{\partial \rho A}{\partial t} + \frac{\partial \rho U A}{\partial z} = 0 \tag{2.46}$$

$$\frac{\partial \rho U A}{\partial t} + \frac{\partial \rho U^2 A}{\partial z} + A\frac{\partial (P + \frac{B^2}{2\mu_0})}{\partial z} = AS2 \tag{2.47}$$

$$\frac{\partial \rho \alpha A}{\partial t} + \frac{\partial \rho \alpha U A}{\partial z} = Am_i S1 \tag{2.48}$$

$$\frac{\partial \rho \alpha T_e A}{\partial t} + \frac{\partial \rho \alpha U T_e A}{\partial z} + \frac{2}{3}\rho \alpha T_e \frac{\partial UA}{\partial z} = A\frac{2}{3}\frac{m_i}{k} S3_e \tag{2.49}$$

$$\frac{\partial \rho T_g A}{\partial t} + \frac{\partial \rho U T_g A}{\partial z} + \frac{2}{3}\rho T_g \frac{\partial UA}{\partial z} = A\frac{2}{3}\frac{m_i}{k} S3_g \tag{2.50}$$

$$\frac{\partial BA}{\partial t} + \frac{\partial UBA}{\partial z} + \frac{1}{\sigma \mu_0}\left(\frac{A}{\sigma}\frac{\partial \sigma}{\partial z} - \frac{\partial A}{\partial z}\right)\frac{\partial B}{\partial z} = \frac{A}{\sigma \mu_0}\frac{\partial^2 B}{\partial z^2} \tag{2.51}$$

2.6 Vector Formulation

The governing equations can be written in the form

$$\frac{\partial VA}{\partial t} + \frac{\partial gA}{\partial z} + h(V)\frac{\partial UA}{\partial z} + k(V)\frac{\partial V}{\partial z} + Al(V)\frac{\partial^2 V}{\partial z^2} + AS = 0 \tag{2.52}$$

where

$$V = \begin{bmatrix} \rho \\ \rho U \\ B \\ \rho \alpha \\ \rho \alpha T_e \\ \rho T_g \end{bmatrix} \quad g = \begin{bmatrix} \rho U \\ \rho U^2 \\ UB \\ \rho \alpha U \\ \rho \alpha T_e U \\ \rho T_g U \end{bmatrix} \quad h = \begin{bmatrix} 0 \\ 0 \\ 0 \\ 0 \\ \frac{2}{3}\rho \alpha T_e \\ \frac{2}{3}\rho T_g \end{bmatrix}$$

$$k = \begin{bmatrix} 0 \\ 0 \\ \frac{1}{\sigma \mu_0}\left(\frac{A}{\sigma}\frac{\partial \sigma}{\partial z} - \frac{\partial A}{\partial z}\right) \\ 0 \\ A\frac{\partial K_e}{\partial z} \\ 0 \end{bmatrix} \quad l = \begin{bmatrix} 0 \\ 0 \\ \frac{-1}{\mu_0 \sigma} \\ 0 \\ -K_e \\ 0 \end{bmatrix} \quad S = \begin{bmatrix} 0 \\ S2 + \frac{\partial (P + \frac{B^2}{2\mu_0})}{\partial z} \\ 0 \\ S1_e \\ S3_e - \frac{\partial}{\partial z}\left(K_e \frac{\partial T_e}{\partial z}\right) \\ S3_g \end{bmatrix} \tag{2.53}$$

They are written in this form to facilitate programming the numerical method for the computer.

2.7 Boundary Conditions

2.7.1 Inlet

A number of the inlet boundary conditions are given by the physical characteristics of the flow. These boundary conditions are the total mass flow per unit area, $\frac{\dot{m}}{A} = \rho U$ and the total enthalpy, $h_{t0} = \frac{\gamma P}{\rho(\gamma-1)} + \frac{1}{2}U^2 + \alpha\frac{E_i}{m_i}$. The mass flow per unit area was chosen to be 0.5 $\frac{kg}{m^2 \cdot s}$. For a thruster with concentric electrodes and an inner electrode radius of 9 cm, similar to the experimental device of Heimerdinger and Kilfoyle [4], this corresponds to a mass flow of 4.7 g/s, close to their mass flow of 4 g/s. Also, the magnetic field at the inlet is determined by the applied current, $B_0 = \frac{\mu_0 I}{D}$. The inlet ionization fraction is assumed to be constant and small, equal to 0.01. The inlet ionization should really be zero. However, the model being used in this research does not allow for ionization to begin in a fluid with zero ionization. Therefore, the ionization fraction is chosen to be small enough so that it will, presumably, have no effect on the bulk of the flow. The validity of this assumption is tested in Section 5.1. The heavy species temperature at the inlet is also assumed to be constant and equal to room temperature, 300 K. The total inlet enthalpy is assumed to be $2.1 \times 10^5 \frac{m^2}{s^2}$ in the one fluid cases, and $5.5 \times 10^5 \frac{m^2}{s^2}$ in the two fluid cases, to allow for the inlet ionization.

For cases without electron heat conduction the inlet density is found by a downwind difference, a one sided finite difference formulation of the overall continuity equation at the zeroth point (i = 0),

$$\rho_0^{n+1} = \rho_0^n - \frac{\Delta t}{2A_0\Delta x}(-3\rho_0^n U_0^n A_0 + 4\rho_1^{n+1}U_1^{n+1}A_1 - \rho_2^{n+1}U_2^{n+1}A_2) \tag{2.54}$$

Once the density at the inlet is known, the velocity can be found from the mass flow. Then, the pressure can be computed from the total enthalpy. The electron temperature can then be computed as a function of the other known variables. For cases with electron heat conduction, the electron temperature is assumed to be the same as that at the next inside point, and the density is then found as a function of the other known quantities.

2.7.2 Outlet

At the outlet it is assumed that if the flow is supersonic, the variables at the exit, denoted by the subscript n, are set equal to the variables at the closest inside point, n-1, with the exception of the magnetic field, the pressure, and the gas temperature, which are given by

$$
\begin{aligned}
B_n &= 0 \\
P_n &= P_{n-1} + \frac{B_{n-1}^2}{2\mu_0} \\
T_{g_n} &= \frac{kP_n}{m_i \rho_n} - \alpha_n T_{e_n}
\end{aligned}
\tag{2.55}
$$

If the flow is subsonic, the fluid variables ρ and U are given by the Riemann invariants, while P is determined by the external pressure,

$$
\begin{aligned}
P_n &= P_{external} \\
\rho_n &= (\frac{P_n}{\gamma P_{n-1}^*})^{\frac{1}{\gamma}} \rho_{n-1} \\
U_n &= U_{n-1} + \frac{2}{\gamma - 1}(a_{n-1} - a_n)
\end{aligned}
\tag{2.56}
$$

where $a_j = \sqrt{\frac{\gamma P_j^*}{\rho_j}}$, $P_j^* = P_j + \frac{B_j^2}{2\mu_0}$, and $P_{external}$ is chosen to be some very small pressure. The electron temperature and ionization fraction are again taken from the inside point, n-1, and the heavy species temperature is then computed as in the supersonic case.

2.8 Initial Conditions

Initial conditions were chosen to be close to the steady state solution. The massflow was chosen to be constant, with a cosine distribution for the velocity. The initial current distribution was constant, as was the electron temperature, the ionization fraction, and the pressure.

2.9 One Fluid Model

In order to test the methods used in this research a one fluid model was also studied. For the one fluid model comparisons could be made to existing results, as in Martinez [10]. The one fluid equations are the same as the two fluid set, with

$$
\begin{aligned}
\alpha &= 1 \\
T_g &= 0 \\
P &= nkT_e
\end{aligned}
$$

and all the source terms, except for $\frac{J^2}{\sigma}$ set to zero. The results for this model, and a comparison with previous results, are given in Chapter 4.2.

2.10 Performance Calculations

The thrust produced by any device can be obtained by drawing a control volume around the device and examining the forces acting on it. As the exit magnetic field is zero, the thrust produced is given by

$$T = \dot{m}U_n + P_n A_n \tag{2.57}$$

where the subscript n represents the value at the exit. The thrust per unit throat area is then given by

$$\tilde{T} = (\rho_n U_n^2 + P_n)\frac{A_n}{A_t} \tag{2.58}$$

where the subscript t represents the value at the throat. The jet power produced by the thruster is given by

$$W_{out} = \frac{1}{2}\frac{T^2}{\dot{m}} \tag{2.59}$$

As the input power is simply the product IV, where the potential V is EH, the efficiency is the ratio of the power produced to the input power,

$$\eta = \frac{1}{2}\frac{\mu_0 \tilde{T}^2}{\rho_n U_n B_0 E_t} \tag{2.60}$$

Chapter 3

Numerical Method

3.1 Overall Scheme

As shown in equation 2.52, all of the differential equations comprising the model developed previously can be written in the form

$$\frac{\partial V}{\partial t} + \frac{\partial g}{\partial z} + h(V)\frac{\partial U}{\partial z} + k(V)\frac{\partial V}{\partial z} + l(V)\frac{\partial^2 V}{\partial z^2} + S = 0 \tag{3.1}$$

where the vectors are as given in the previous chapter. These equations include diffusive terms, convective terms, and source terms. Each type of term has its own time scale which limits the maximum time step allowed for a finite difference representation of that term. For example, for a purely convective equation, of the form,

$$V_t + (UV)_z = 0 \tag{3.2}$$

the time limit for an explicit finite difference scheme is given by the Courant-Fredrichs-Lowy condition

$$\Delta t_c = \frac{\Delta z}{U} \tag{3.3}$$

For a diffusive equation, where

$$V_t + l(V)(V)_{zz} = 0 \tag{3.4}$$

the maximum time step for an explicit method is of the form

$$\Delta t_d = \frac{(\Delta z)^2}{l(V)} \tag{3.5}$$

These two time scales can be very different. The ratio between them is given by

$$N = \frac{\Delta t_c}{\Delta t_d} = \frac{l(V)}{U\Delta z} \tag{3.6}$$

For magnetic diffusion and electron heat conduction, this ratio can vary from 2 to 20,000. To integrate all of the equations with the time step given by the diffusive limit would

neccesitate performing many more iterations than for a purely convective system of equations. To get around this problem, the magnetic field equation is integrated separately from the other equations, as is the diffusive part of the electron temperature equation. The convective part of the electron temperature equation is integrated with the other convective equations because of the interdependence between all of the fluid equations. Also, the non conservative terms in the temperature equations are evaluated with a centered space approximation and lumped in with the source terms. In addition, some numerical methods are more suited for one type of equation than another, so more than one type of method is used even for the convective equations. The overall numerical scheme is as follows:

1. Evaluate all of the source terms using the values of the variables at the previous time step, including the U_z terms, evaluated by
$$U_z = \frac{U^n_{j+1} - U^n_{j-1}}{2\Delta z} \tag{3.7}$$
2. Integrate the magnetic field equation, the fast equation, N times, where N is as given in equation 3.6, holding all other variables constant. The magnetic field integration is done using McCormack's method, described in Section 3.4.
3. Integrate the convective terms of the fluid equations using Rusanov's method, described in Section 3.2, for the overall density and momentum equations, and the Donor Cell method, described in Section 3.3, for the electron density and species temperature equations. Both methods are of the form
$$V^{n+1}_j = V^n_j - \frac{\Delta t}{\Delta x}(G^n_j - G^n_{j-1}) \tag{3.8}$$
4. Add in the contribution from the source terms.
5. Integrate the diffusive part of the electron temperature equation, again using McCormack's method. The maximum time step for this integration is reevaluated at every iteration of the overall method.

3.2 Modified Rusanov Method

Rusanov's method was developed by V. Rusanov [16]. It is a modification of the Lax method, where V(i,j) is replaced by an average of V over adjacent points. The fluxes for this method are given by
$$G_{j+\frac{1}{2}} = \frac{1}{2}(g_j + g_{j+1}) - \frac{|U_j + U_{j+1} + a_j + a_{j+1}|}{4}(V_{j+1} - V_j) \tag{3.9}$$

where

$$a_j = \sqrt{\frac{\gamma P_j^*}{\rho_j}} \tag{3.10}$$

The flow examined in this study varies from low velocity at the inlet to very high velocities at the exit. At the inlet, the artificial damping introduced by the Rusanov scheme outweighs the physical fluxes. To remove this problem, the damping terms are multiplied by the ratio of the local velocity to the inlet magnetic velocity, $U_{mag} = \frac{B_0^2 A}{2\mu_0 \dot{m}}$.

3.3 Donor Cell Scheme

The donor cell scheme is another low order scheme, particularly suited for purely convective equations. In this study it was used to integrate the equations for the ionization fraction, the electron temperature, and the the heavy species temperature. The fluxes for this method are given by

$$G_j = U_r V_r \tag{3.11}$$

where

$$U_r = \frac{U_{j+1} + U_j}{2} \tag{3.12}$$

$$V_r = \begin{cases} V_j & \text{if } u_r > 0 \\ V_{j+1} & \text{if } u_r \leq 0 \end{cases} \tag{3.13}$$

3.4 McCormack's Method

The magnetic field equation and the heat conduction part of the the electron temperature equation contain both diffusive and convective terms. McCormack's method, described in Anderson et al. [1], is used for the magnetic field equation and the heat conduction terms of the electron temperature equation. The McCormack scheme consists of a predictor step

$$V_j^{\overline{n+1}} = V_j^n - \frac{\Delta t}{\Delta x}(g_{j+1}^n - g_j^n) - k_j^n \frac{\Delta t}{\Delta x}(V_{j+1}^n - V_j^n) - l_j^n \frac{\Delta t}{\Delta^2 x}(V_{j+1}^n - 2V_j^n + V_{j-1}^n) \tag{3.14}$$

and a corrector step

$$V_j^{n+1} = \frac{1}{2}[V_j^n + V_j^{\overline{n+1}} - \frac{\Delta t}{\Delta x}(g_j^{\overline{n+1}} - g_{j-1}^{\overline{n+1}}) + k_j^n \frac{\Delta t}{\Delta x}(V_j^{\overline{n}} - V_{j-1}^{\overline{n}}) - l_j^n \frac{\Delta t}{\Delta^2 x}(V_{j-1}^{\overline{n+1}} - 2V_j^{\overline{n+1}} + V_{j-1}^{\overline{n+1}})] \tag{3.15}$$

For the heat conduction of the electron temperature equation, $g = 0$, $k = \frac{\partial K_e}{\partial z}$, and $l = K_e$. For the magnetic field equation, $g = UB$, $k = \frac{1}{\sigma^2 \mu_0} \frac{\partial \sigma}{\partial z}$ and $l = \frac{1}{\mu_0 \sigma}$. This scheme is second order accurate for both the space and time derivatives.

Chapter 4

One Fluid Results

4.1 Steady State

Although the numerical methods used in this research are unsteady methods, all of the results shown are steady state results. Steady state was assumed to occur when the mass flow at any point differed by less than 1% from the inlet mass flow. For the time steps used in these calculations, with Courant number ranging from 0.1 to 0.3, steady state was reached after 10,000 to 20,000 steps, around 20 to 40 minutes of computer time.

4.2 Nondimensional Results

As described in Section 2.9, it is possible to solve the one fluid equations with the method developed for the two fluid equations. The one fluid case therefore served as a valuable test for the method, because, as described in Chapter 1, it has already been analyzed by others. Martinez [10] and Sheppard [17] both used a space marching method to find the steady state solution to the one fluid equations. Both references use equations where the inlet magnetic field, B_0, the massflow, $\dot{m}$, the throat area, A^*, and the channel length L, have been used to nondimensionalize the equations. When written in their nondimensional form, it becomes clear that the governing parameters of the model are the magnetic Reynold's number, R_{mag}, defined by

$$R_{mag} = \mu_0 U_{ref} \sigma L \tag{4.1}$$

and the inlet total enthalphy, h_{t0}. Using these non dimensional variables, the final steady state results for two values of the magnetic Reynolds number were obtained. They are given in Figures 4.1 and 4.2. A R_{mag} of 4.9258 is chosen to facilitate comparisons with Martinez's results for that value of R_{mag}. The results from Sheppard for R_{mag} = 4.9258 and 20 are shown in Figures 4.3 and 4.4, respectively. As both references used a constant

$P_{ref} = \frac{B_0^2}{2\mu_0}$	$U_{ref} = \frac{B_0^2 A^*}{2\mu_0 \dot{m}}$
$z_{ref} = L$	$B_{ref} = B_0$
$\rho_{ref} = \frac{2\mu_0}{B_0^2}(\frac{\dot{m}}{A^*})^2$	$E_{ref} = \frac{B_0^3}{2\mu_0 \dot{m}}$

Table 4.1: Reference Variables

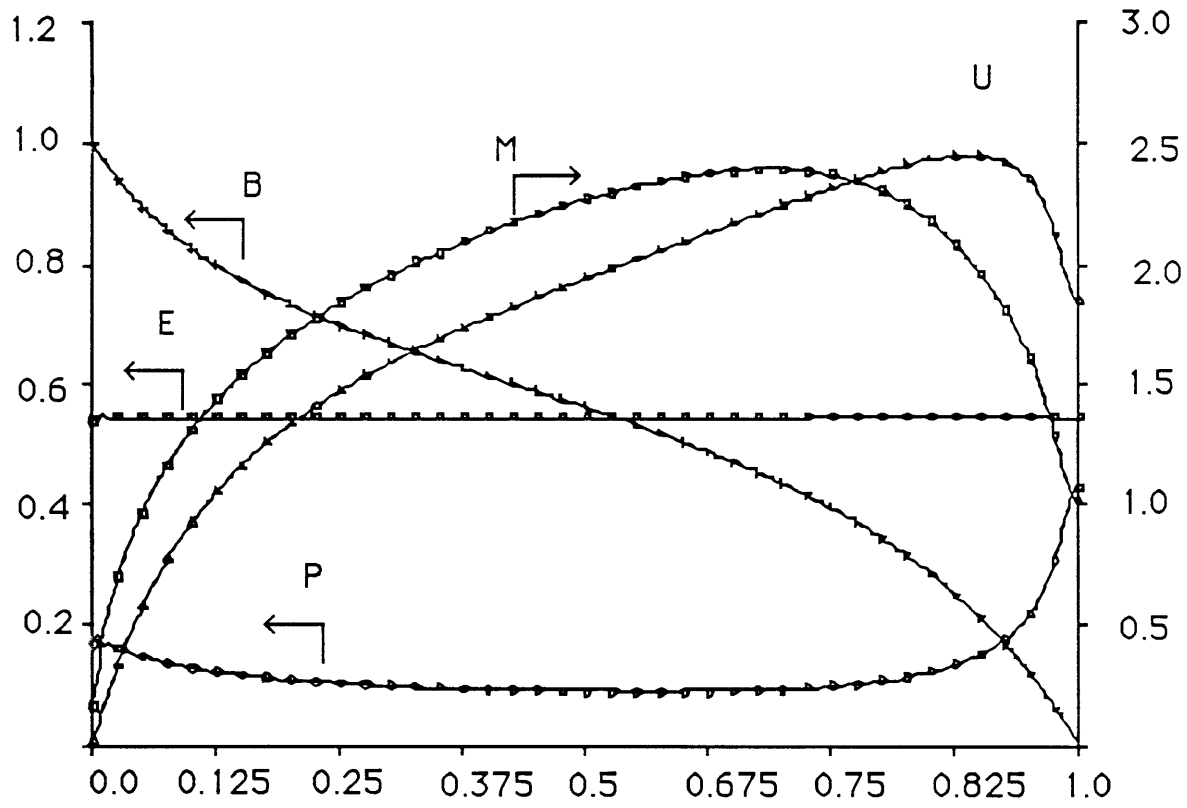

Figure 4.1: One Fluid Results in Nondimensional Variables: R_{mag}= 4.9528

γ of $\frac{5}{3}$ and a nondimensional inlet enthalpy of 0.00328, the same values were chosen for this research. The inlet enthalpy is chosen to represent a cold gas. Both one fluid cases examined with this method give good agreement with the references. A nondimensional electric field of 0.433 for the R_{mag} = 20 and 0.544 for the R_{mag} = 4.9258 was computed. This is quite close to 0.461 and 0.544 found by Sheppard for the two cases, and 0.55 found by Martinez for R_{mag} =4.9258.

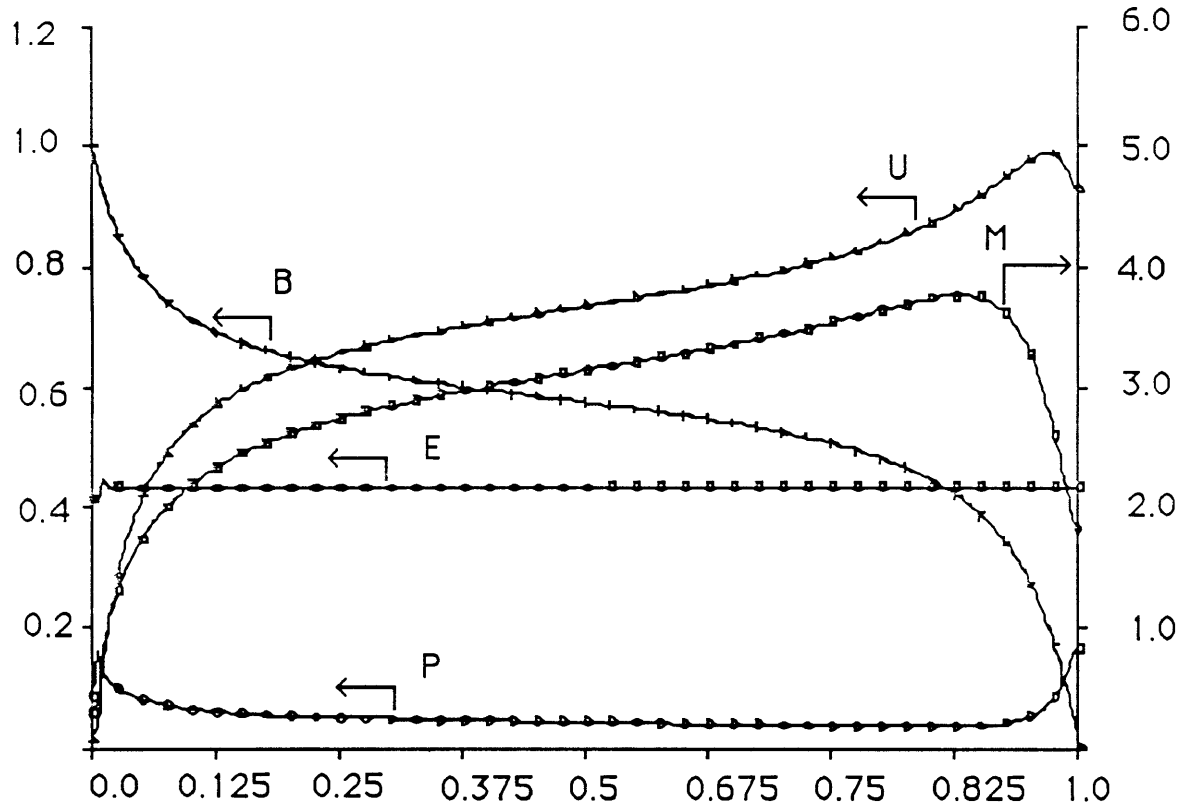

Figure 4.2: One Fluid Results in Nondimensional Variables: R_{mag} = 20.0

$P_{ref} = 3980\ Pa$	$U_{ref} = 7960\ m/sec$
$z_{ref} = 0.2\ m$	$B_{ref} = 0.1\ Tesla$
$\rho_{ref} = 6.28 \times 10^{-5}\ kg/m^3$	$E_{ref} = 796.2\ V/m$

Table 4.2: MKS Values for Reference Variables

4.3 MKS Results

The two fluid results are given in MKS units. In order to provide for a comparison between the one fluid and two fluid results, the one fluid results for $R_{mag} = 4.9258$ are also given in MKS units in figures 4.5 - 4.10. These MKS results are obtained assuming a thruster 20 cm. long with an interelectrode separation of 2 cm. The inlet magnetic field is assumed to be 0.1 T, with a mass flow per unit area of 0.5 $\frac{kg}{m^2 \cdot sec}$. These numbers give a conductivity of 2462 $\frac{1}{\Omega \cdot m}$ or Si. The MKS values of the reference variables are given in Table 4.2.

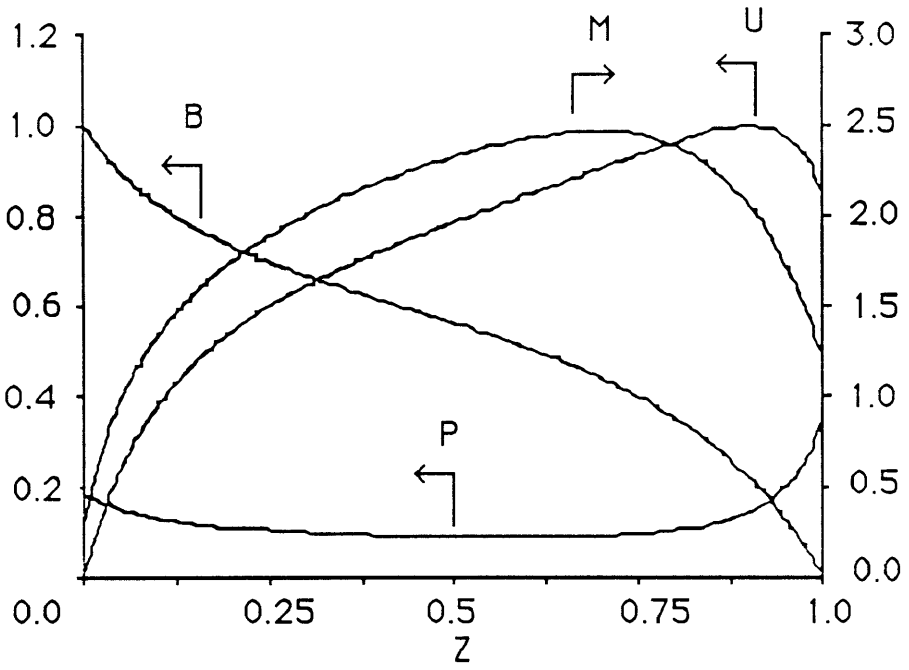

Figure 4.3: Results from Sheppard, R_{mag} = 4.9258

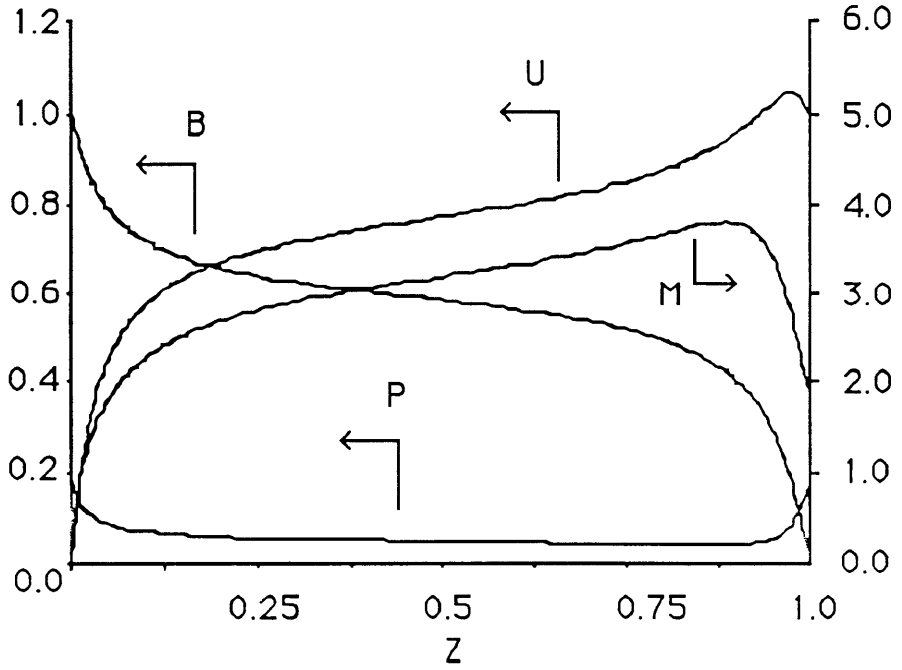

Figure 4.4: Results from Sheppard, R_{mag} = 20.0

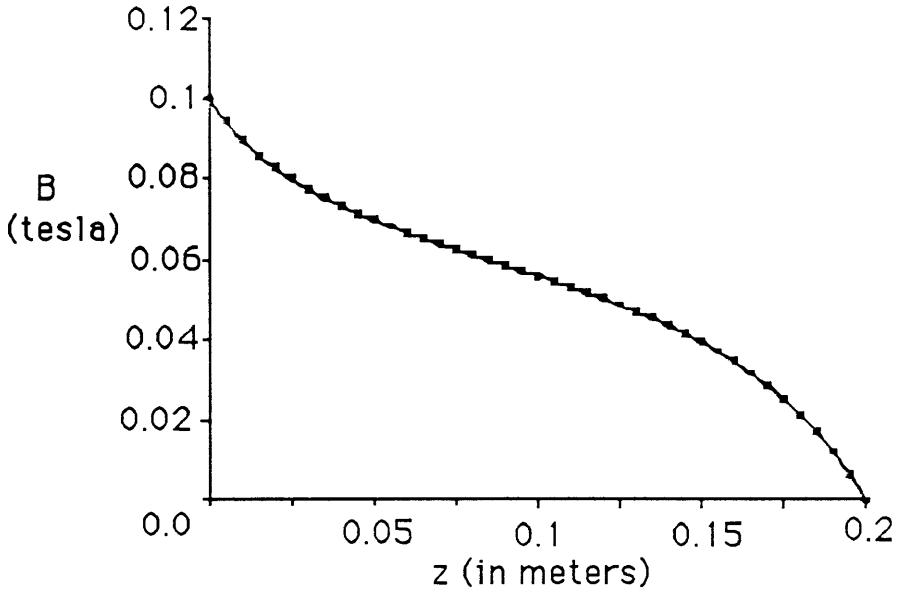

Figure 4.5: Magnetic Field in MKS units for R_{mag} = 4.9258

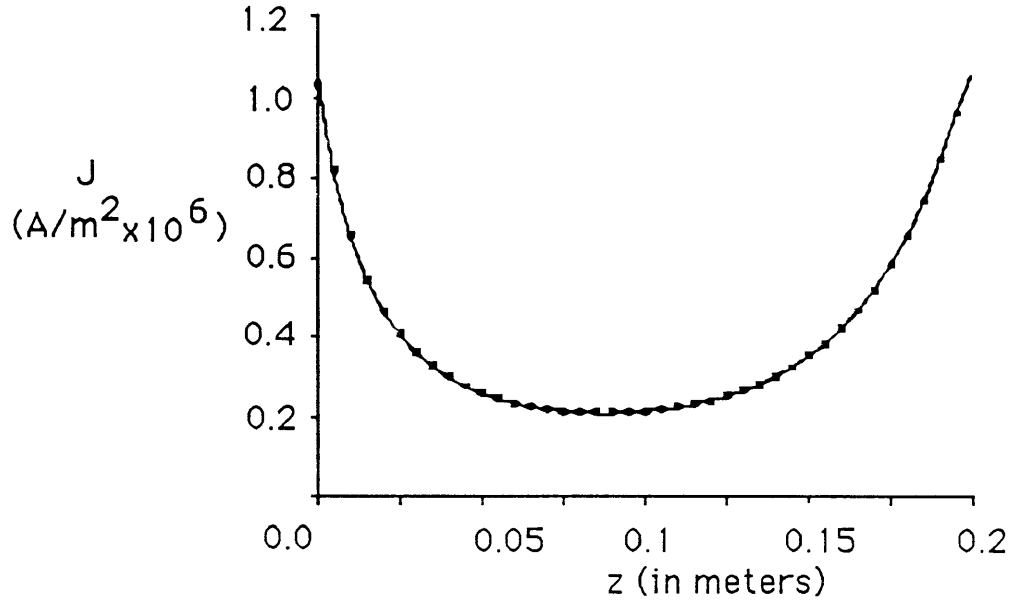

Figure 4.6: Current in MKS units for R_{mag} = 4.9258

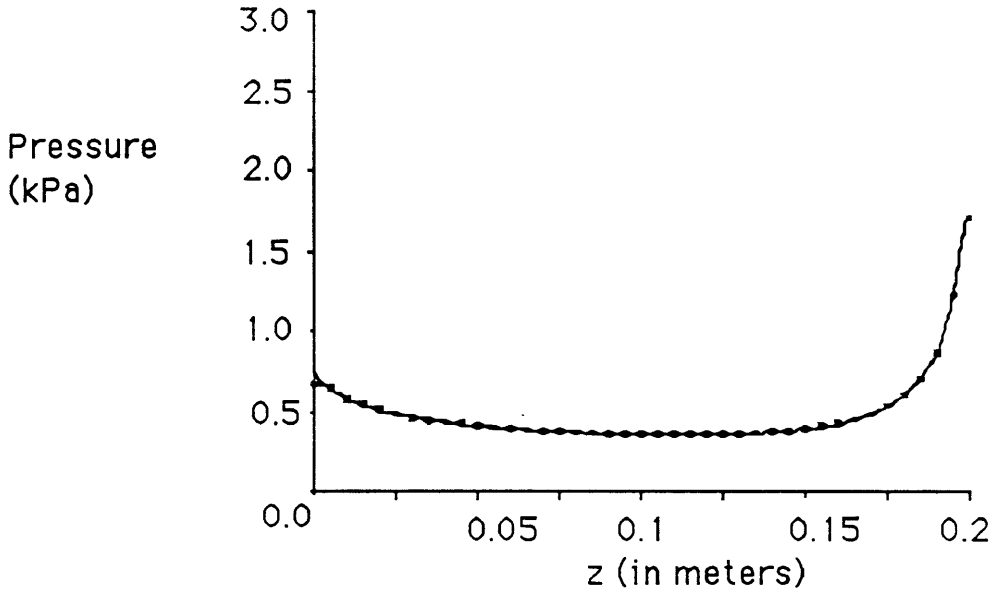

Figure 4.7: Pressure in MKS units for R_{mag} = 4.9258

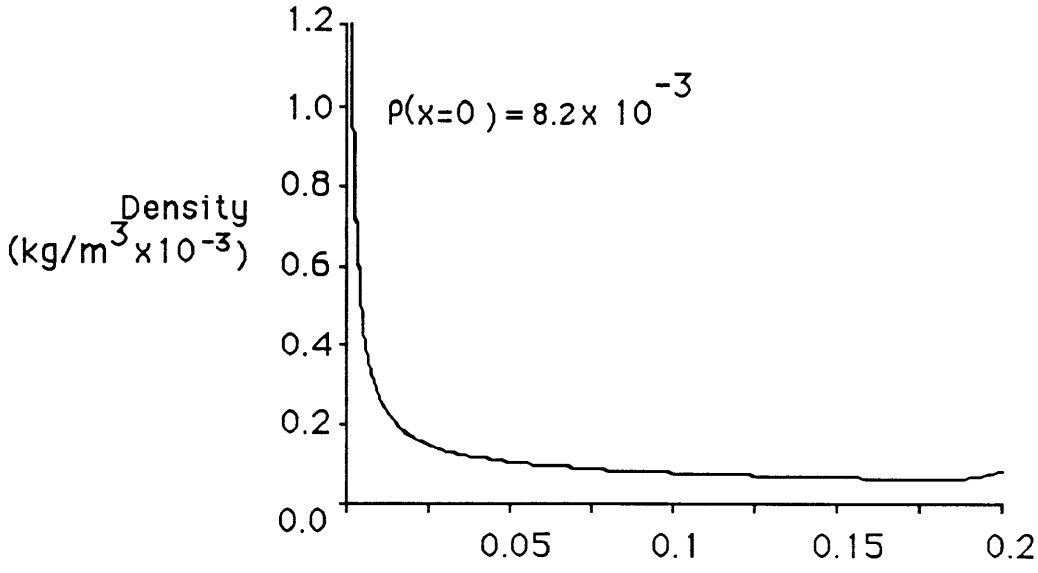

Figure 4.8: Density in MKS units for R_{mag} = 4.9258

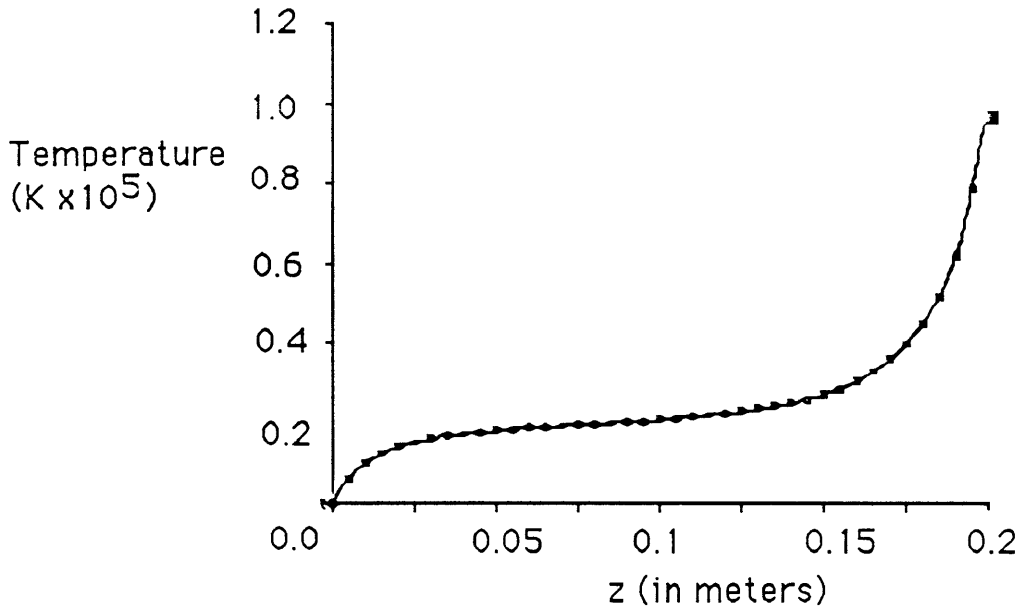

Figure 4.9: Temperature in MKS units for R_{mag} = 4.9258

4.4 Discussion

One noticeable problem with the one fluid results is the fluctuation in electric field at the inlet. This fluctuation is certainly non-physical, as in steady state, from equation 2.20, the electric field is constant in space. The reason for this fluctuation can be understood by examining the McCormack method used to solve the magnetic field equation. In steady state, for $B^{n+1} = B^n$, equation 3.15 gives

$$B_j^{n+1} = B_j^n - \frac{1}{2}[\frac{\Delta t}{\Delta x}(g_{j+1}^n - g_j^n + g_j^{\overline{n+1}} - g_{j-1}^{\overline{n+1}})$$
$$-l_j^n \frac{\Delta t}{(\Delta x)^2}(B_{j+1}^{\overline{n+1}} + B_{j+1}^n - 2B_j^{\overline{n+1}} - 2B_j^n + B_{j-1}^{\overline{n+1}} + B_{j-1}^n)] \tag{4.2}$$

where $g = UB$ and $l = \frac{1}{\mu_0 \sigma}$. Therefore, in steady state , the quantity in the braces is equal to 0. If $B^{\overline{n+1}} = B^n$, then the quantity in braces would be equal to $\frac{\partial E}{\partial z}$, and E would be a constant in space. However, the McCormack method does not guarantee that in steady state $B^{\overline{n+1}} = B^n$, so some error can be introduced in the discretization of equation 2.20.

One other problem with the one fluid results is the small fluctuation in pressure at the inlet. As pressure is not one of the integration variables, differing amounts of damping on the various integration variables which are used to determine the pressure could lead to this problem. This fluctuation does not seem to be present in the two fluid results.

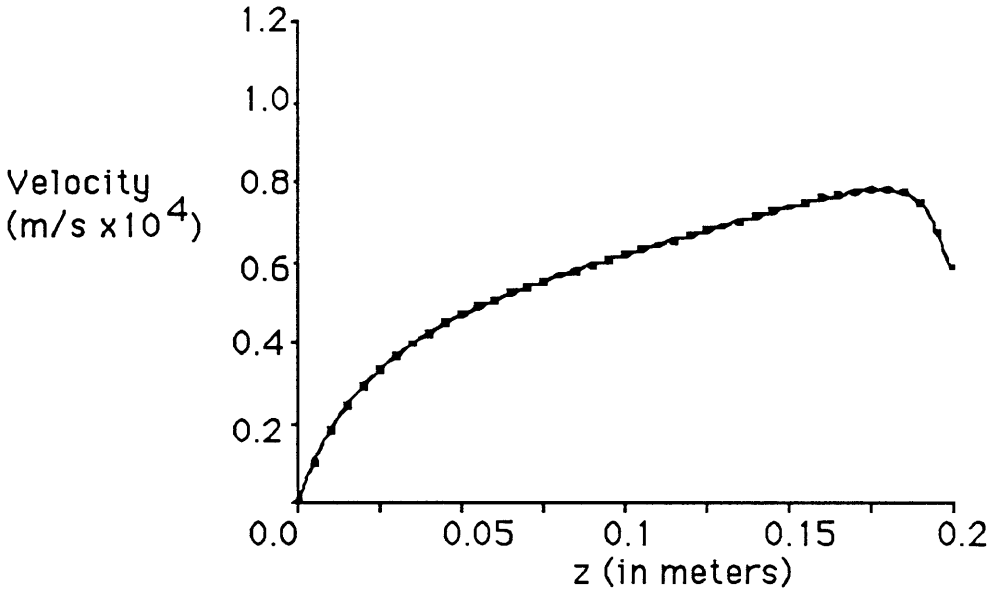

Figure 4.10: Velocity in MKS units for R_{mag} = 4.9258

Chapter 5

Two Fluid Results

5.1 Inlet Ionization

As discussed in Section 2.7.1, the model used in this research does not explain how the fluid, entering the channel with zero ionization, begins to ionize. If the initial ionization was set to zero everywhere, then it would remain zero at all times. To avoid having to model the processes which allow the gas to begin ionization, the inlet ionization is set to some small number, 0.01 in the results discussed later in this chapter and in Chapter 6. To determine the effect of this choice on the flow, two other values for the inlet were chosen and used for a test case. The results for the three values are compared in Figures 5.1 and 5.2, which show the steady state ionization fraction and pressure for the two cases. These figures indicate that as long as a small enough inlet ionization fraction is used, the effect is minimal.

5.2 Inviscid Results

The first attempt at modelling the two fluid equations described in Chapter 2 did not include ambipolar diffusion, viscosity, or heat conduction. The differences between this case and the one fluid cases described earlier are the separate heavy particle and electron temperatures, partial rather than full ionization, and variable conductivity based on the electron temperature. Figures 5.3 - 5.12 show the results for this case, labeled Case 1, in comparison to other cases described later, and, in appropriate figures, to the one fluid results for $R_{mag} = 4.9258$, which has a conductivity similar to this case. Separate results are also given for the electric field, the pressure, and the gas temperature, in Figures 5.13, 5.14 and 5.15, respectively.

One important feature of these results is the large discrepancy between the electron and heavy species temperatures. The heavy species temperature is an order of magnitude

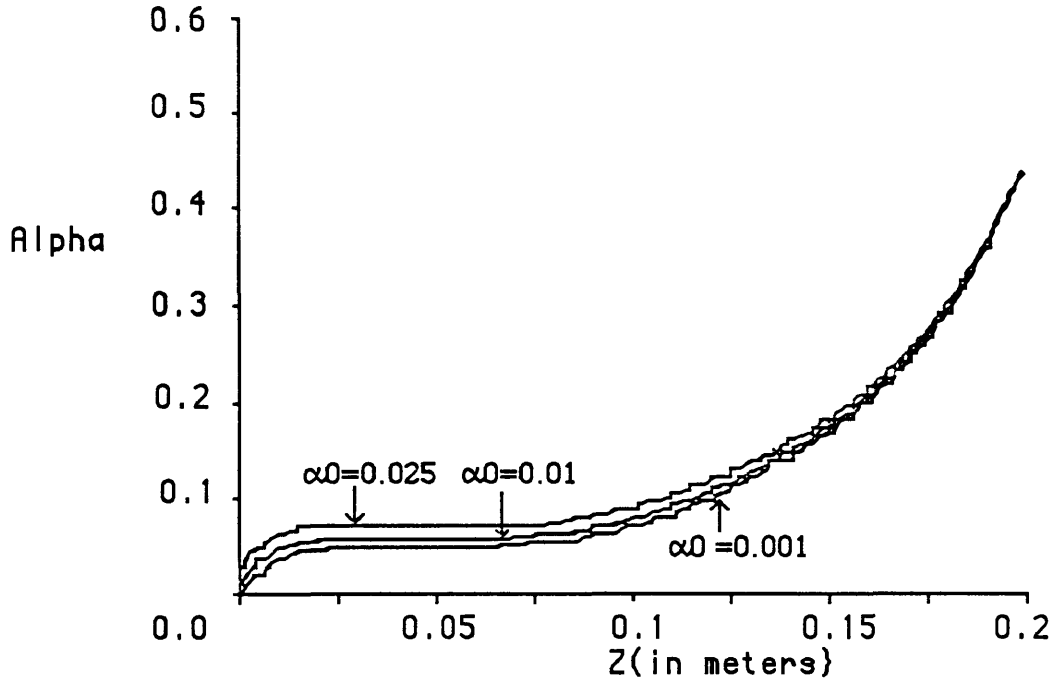

Figure 5.1: Steady State Ionization Fraction for Variations in Inlet Ionization Fraction

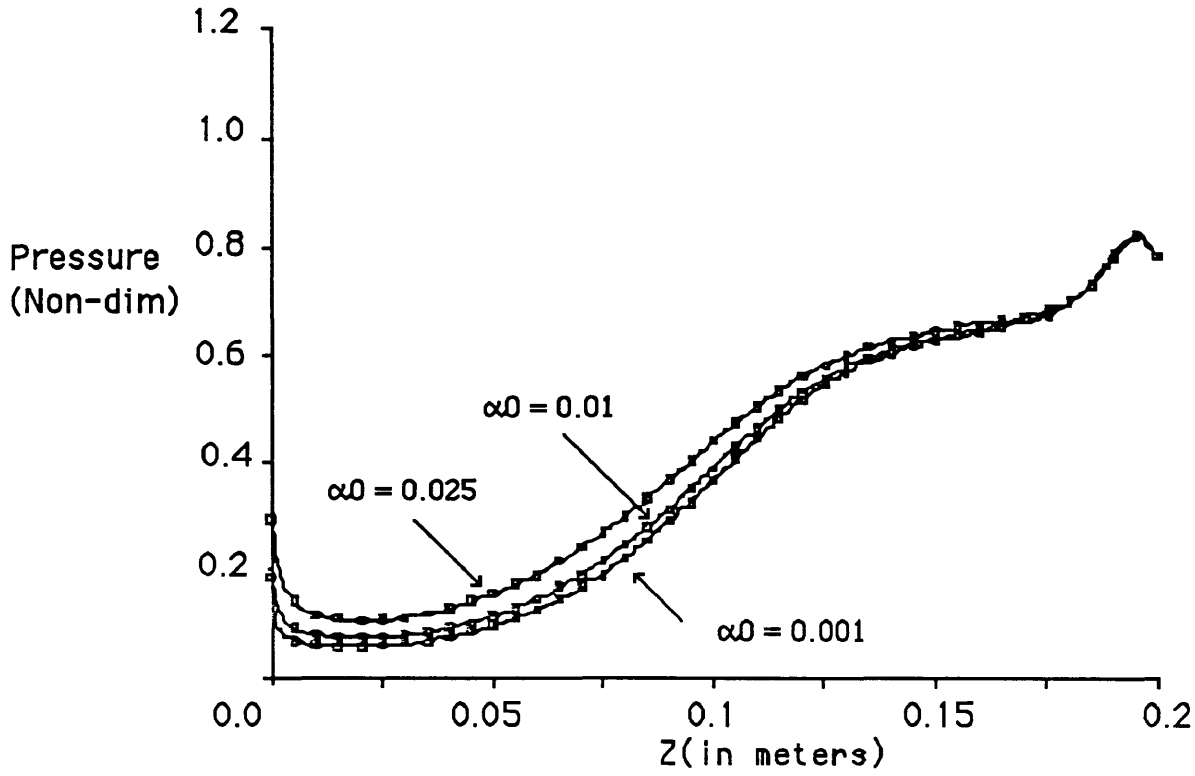

Figure 5.2: Steady State Pressure for Variations in Inlet Ionization Fraction

Interelectrode Seperation: 2 cm	$\frac{\dot{m}}{A^*} = 0.5 \frac{kg}{m^2 \cdot sec}$
Channel Length = 20 cm	B_0 = 0.1 Tesla
T_0 = 300 K	I = $79.6 \frac{kAmp}{m \cdot depth}$

Table 5.1: Thruster Characteristics

smaller than the electron temperature. This would imply that the thermal equilibrium assumed by the one fluid model is not a good assumption. This large difference in temperature arises because there is no effective mechanism in the model of Case 1 for heating the heavy species. The only source term in the heavy species temperature equation, collisional energy transfer with the electrons, is a relatively weak effect. Also, the gas temperature rise at the exit is small, because the ohmic heating all goes into the electrons.

The low heavy species temperature affects the other variables in the model as well. The combination of low ionization fraction, around 0.2 in most of the channel, and low heavy species temperature leads to a lower pressure than in the one fluid case, around 100 Pa rather than 500 Pa. The smaller pressure rise at the exit, partly due to the small increase in gas temperature, prevents the formation of a velocity defect. The velocity continues to rise at the exit, unlike in the one fluid case where there was a drop in velocity at the exit.

There are some other differences between the two cases. The electric field has dropped somewhat from 433.0 V/m in the $R_{mag} = 4.9258$ one fluid case to 399 in this case. The thrust and the efficiency, as given in Table 8.1, have also dropped somewhat.

5.3 Ambipolar Diffusion

The next three sections describe the effect of various additions to the model. The first addition that was made was ambipolar diffusion. As described in Section 2.4, a parabolic distribution is assumed for the electron density. Electrons and ions are absorbed by the wall, and the ionization energy used to create the ionized particles is lost to the walls. The results for this case, labeled Case 2, are shown in Figures 5.3 - 5.12. The electric field for this case is shown in Figure 5.16. The thrust and efficiency are given in Table 8.1. The addition of ambipolar diffusion has caused a sharp decrease in the ionization fraction, and a smaller decrease in the gas temperature. The electron temperature has increased to compensate for the diffusion loss in the ionization fraction. However, it seems to have had little effect on the magnetic field distribution, and hence, the thruster performance. This seems to be because the electrons and ions which are now being lost to the side

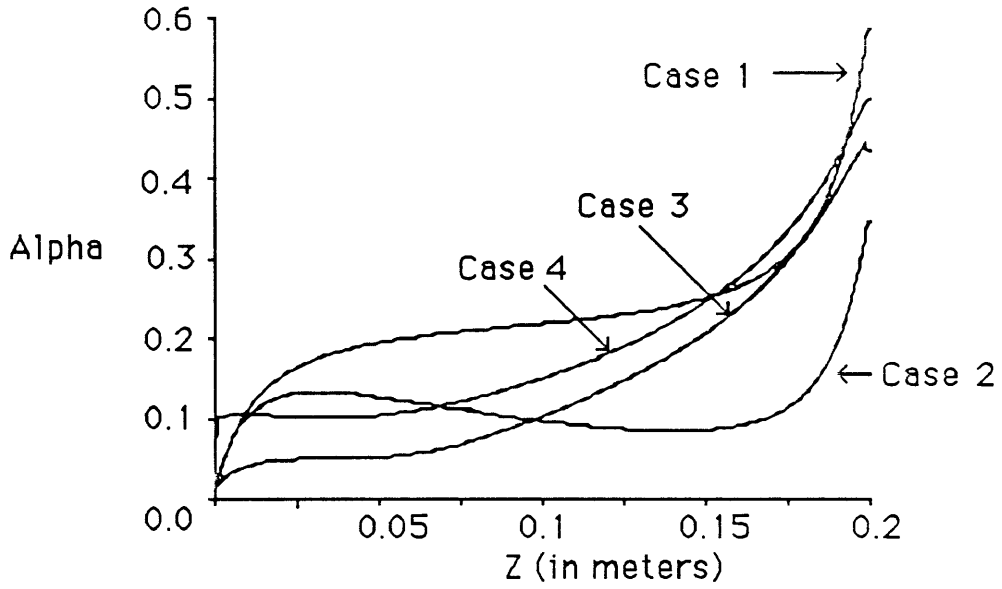

Case 1: No ambipolar diffusion, viscosity, or heat conduction
Case 2: Ambipolar diffusion, but no viscosity or heat conduction
Case 3: Ambipolar diffusion and viscosity, but no heat conduction
Case 4: Ambipolar diffusion, viscosity, and heat conduction

Figure 5.3: Two Fluid Results: Ionization Fraction

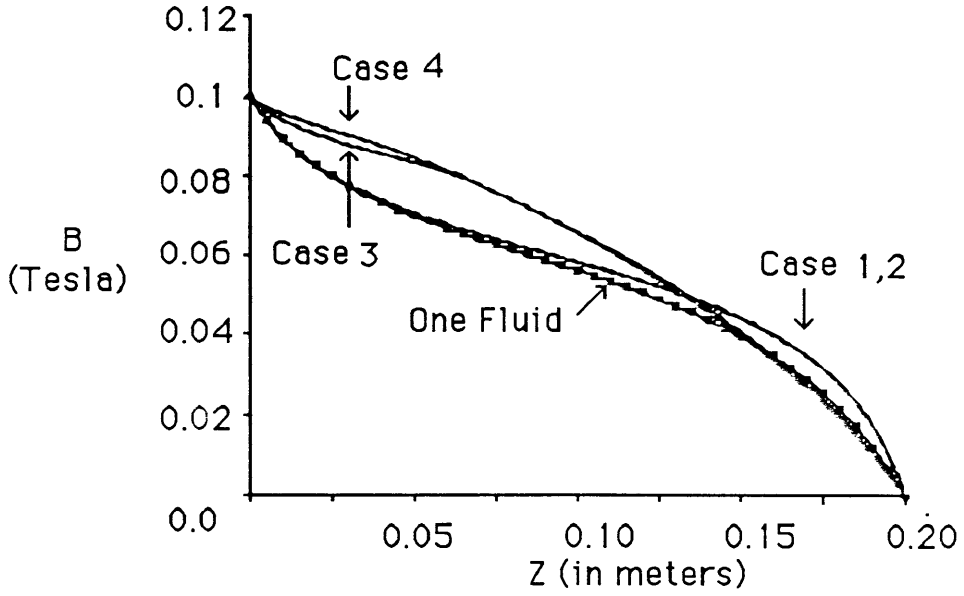

Figure 5.4: Two Fluid Results: Magnetic Field

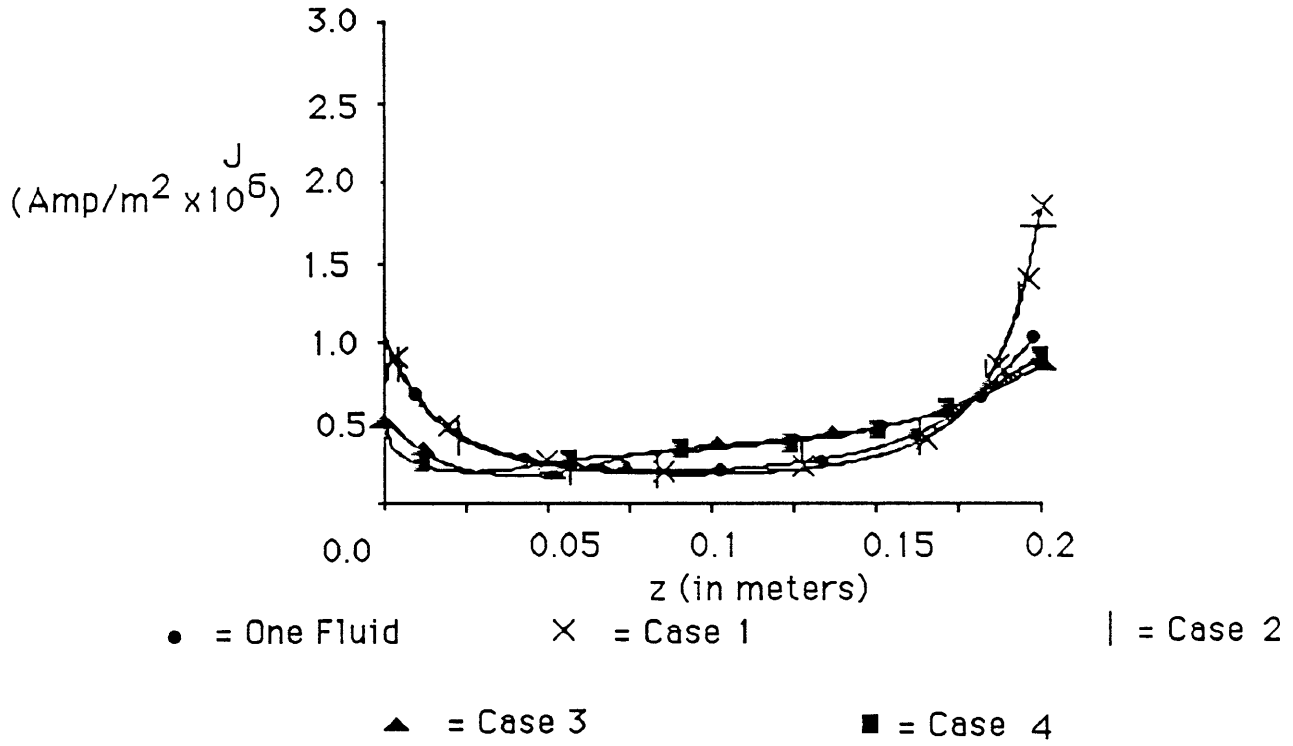

Figure 5.5: Two Fluid Results: Current Density

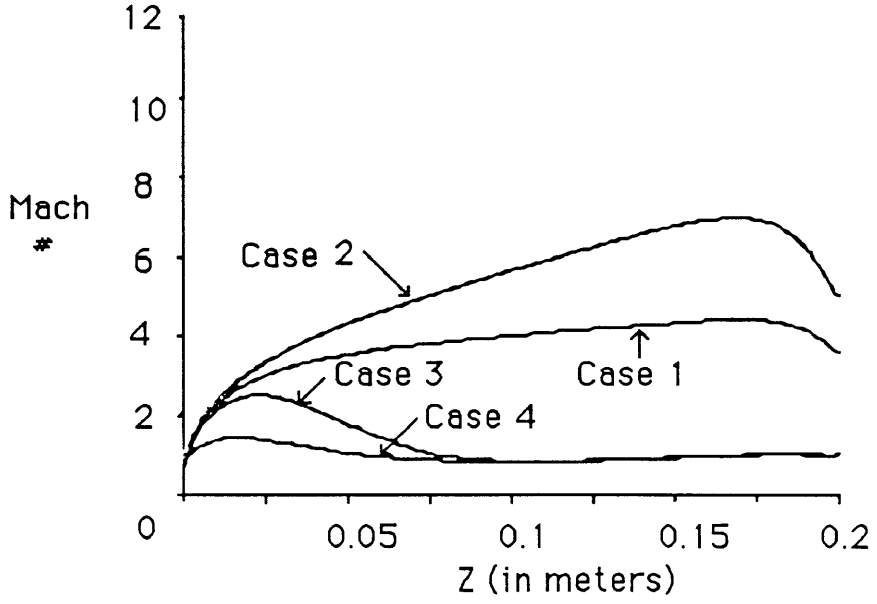

Figure 5.6: Two Fluid Results: Mach Number

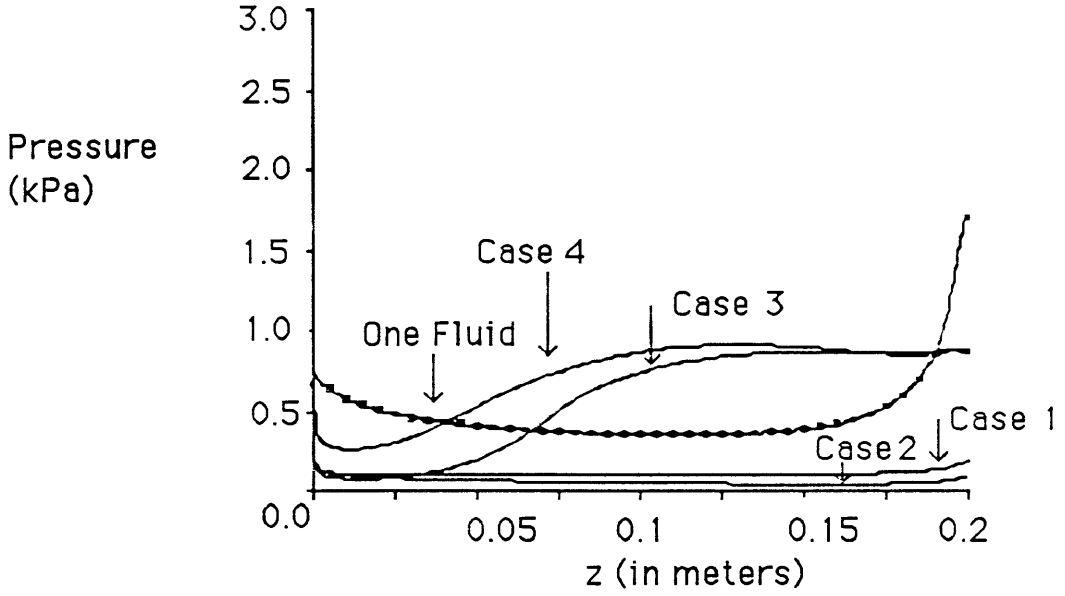

Figure 5.7: Two Fluid Results: Pressure

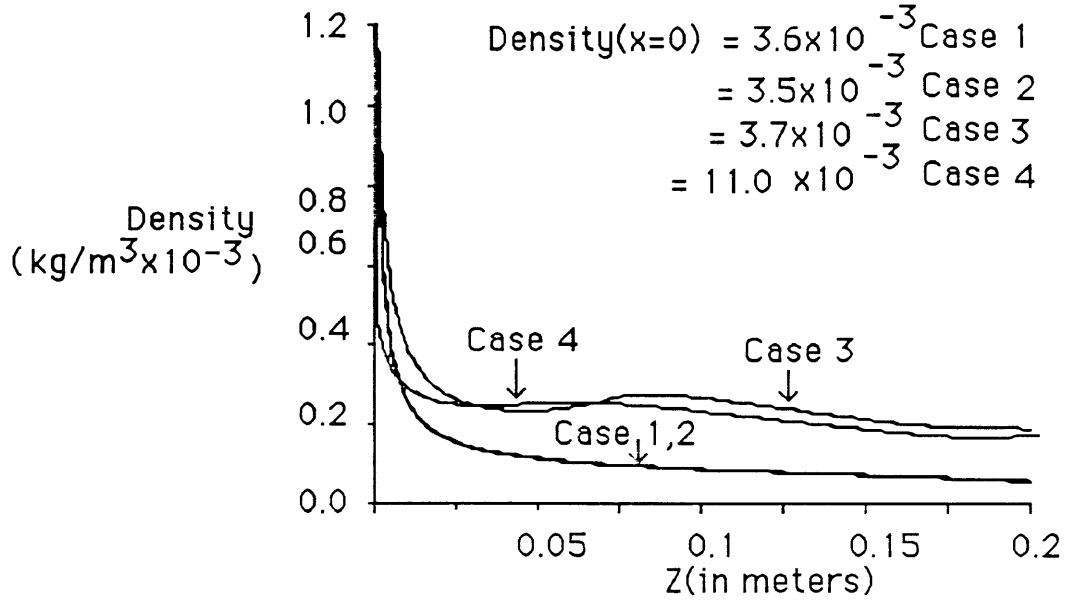

Figure 5.8: Two Fluid Results: Density

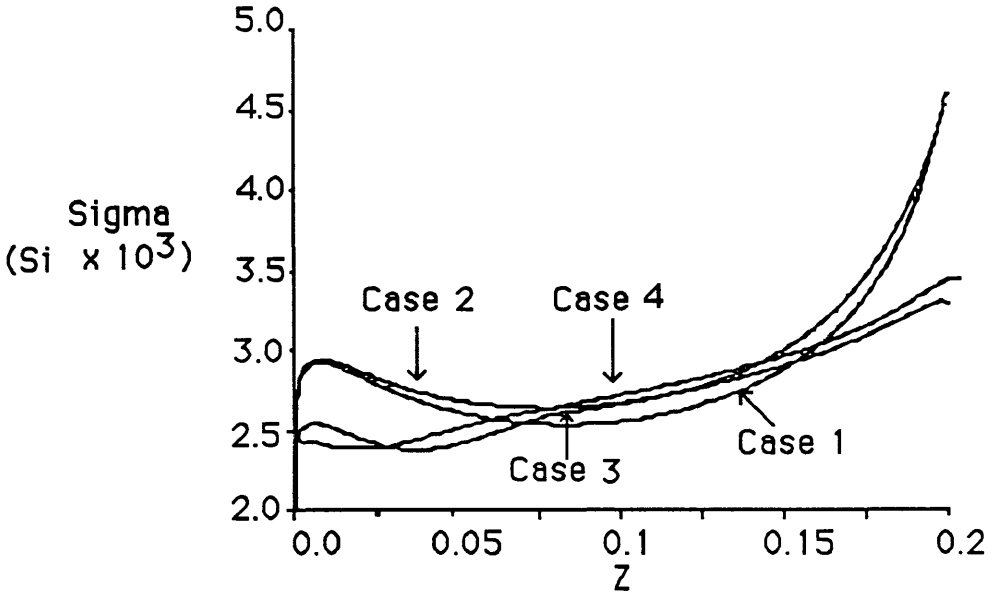

Figure 5.9: Two Fluid Results: Conductivity

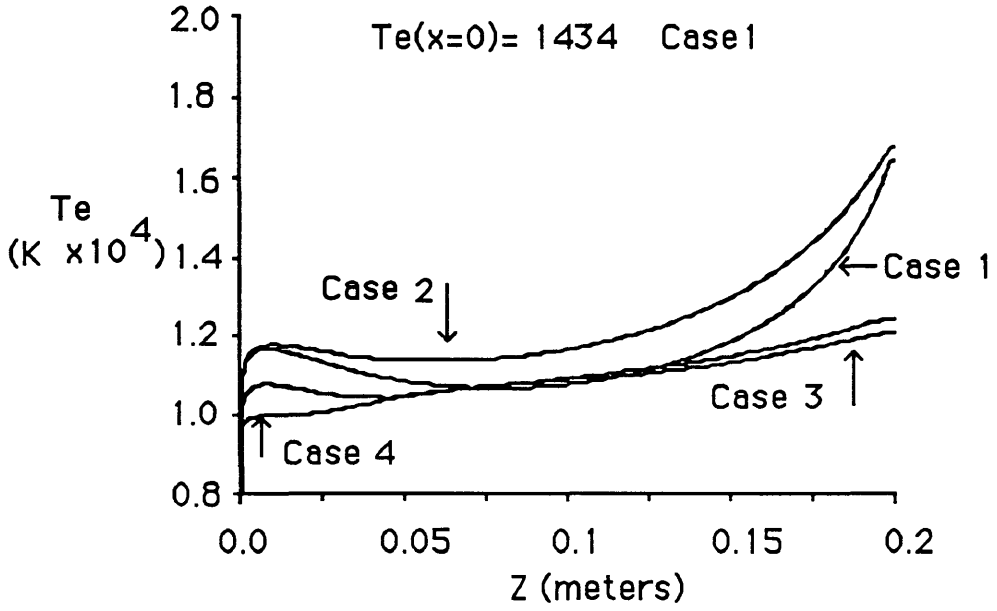

Figure 5.10: Two Fluid Results: Electron Temperature

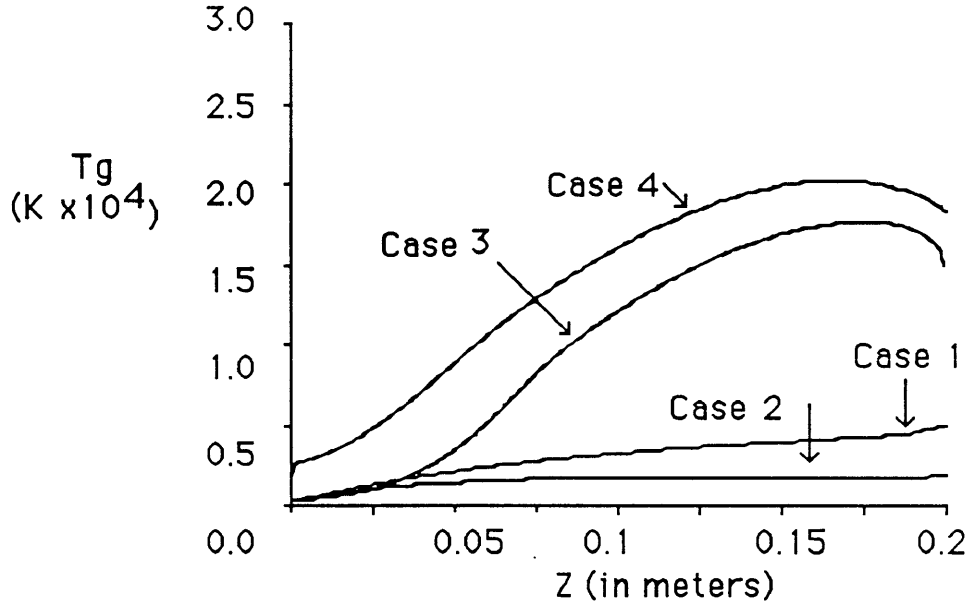

Figure 5.11: Two Fluid Results: Heavy Species Temperature

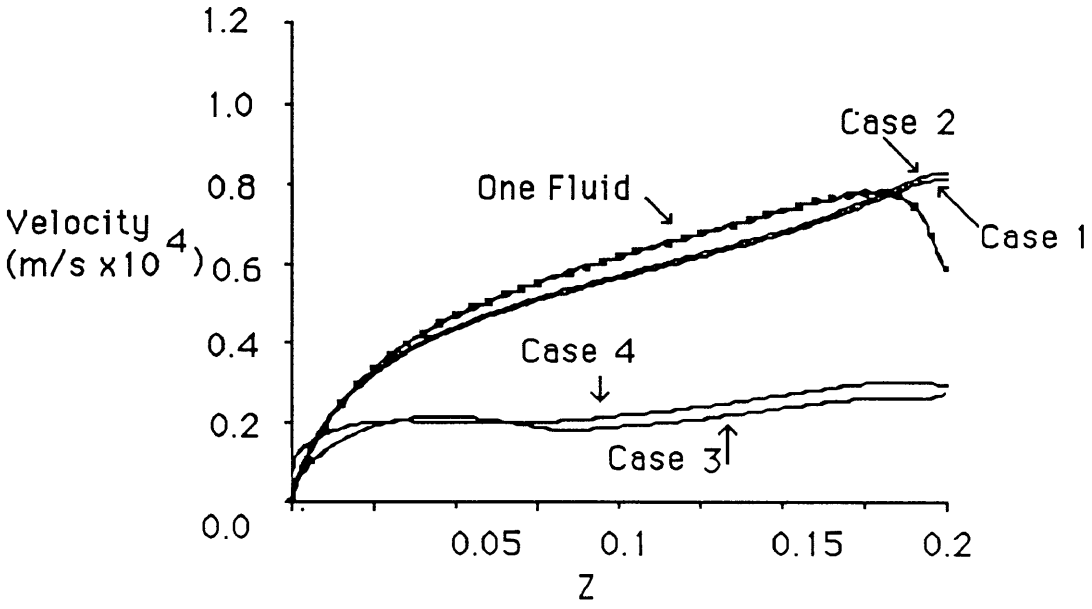

Figure 5.12: Two Fluid Results: Velocity

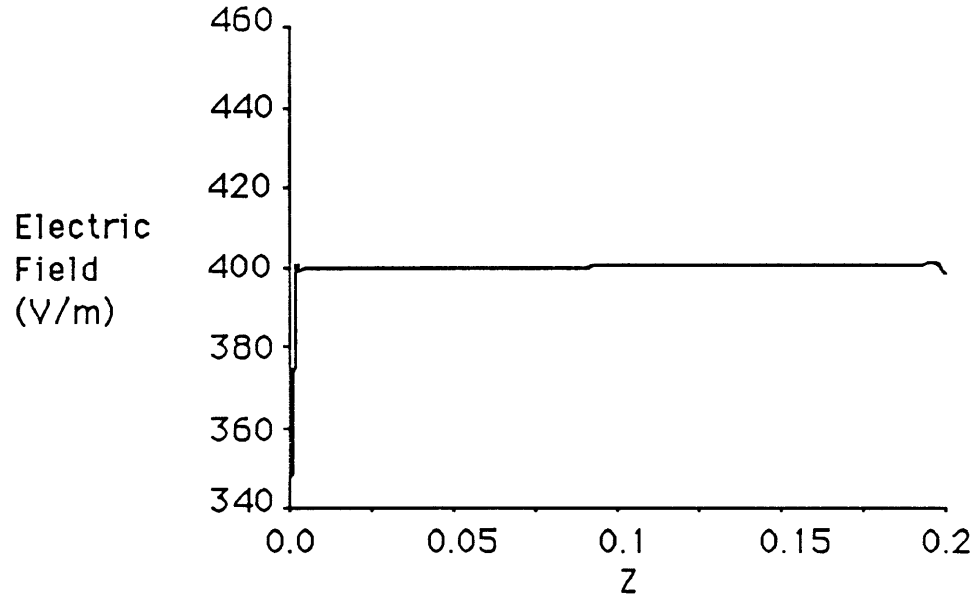

Figure 5.13: Two Fluid Results, Case 1: Electric Field

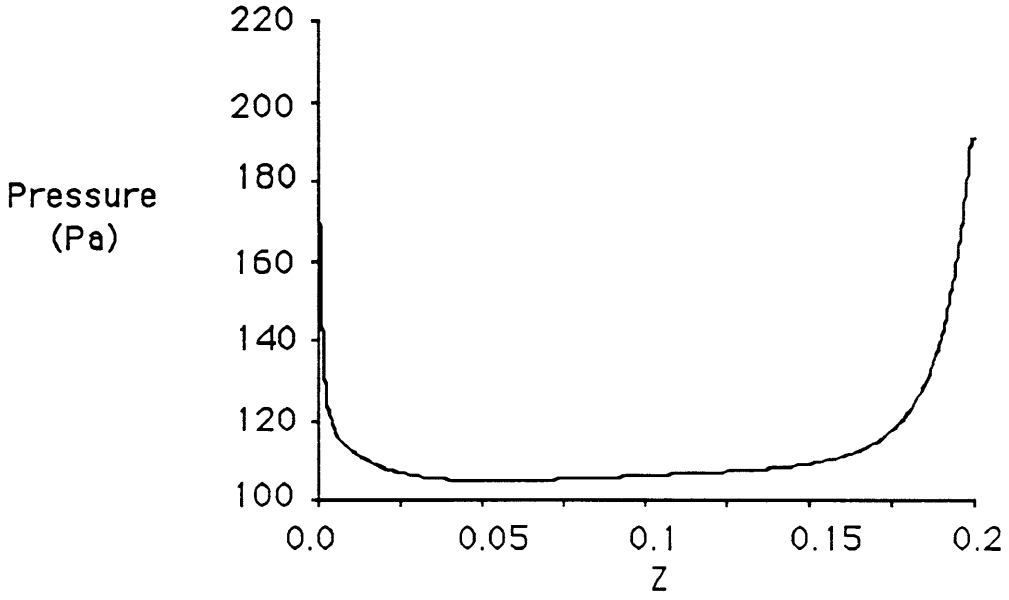

Figure 5.14: Two Fluid Results, Case 1: Pressure

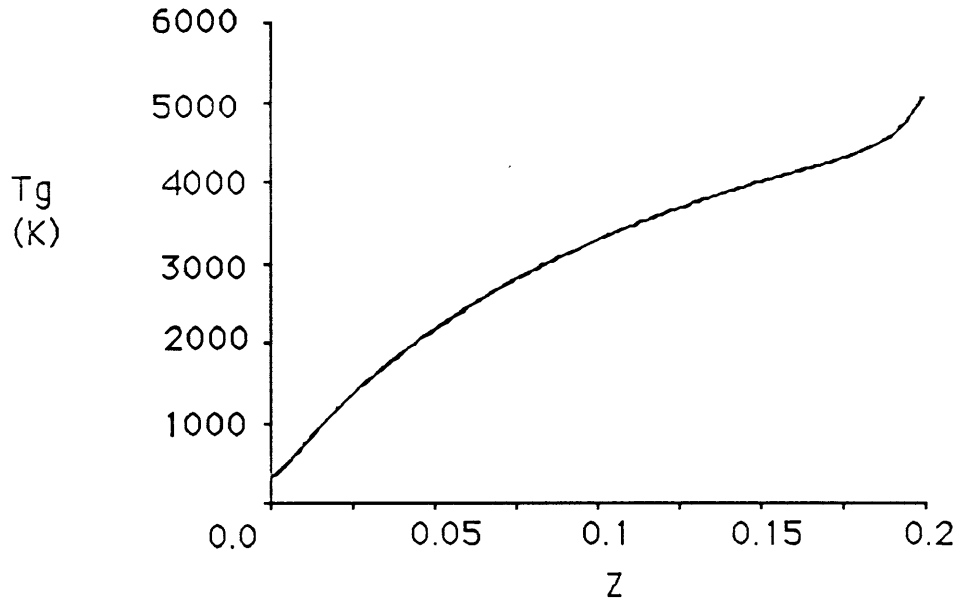

Figure 5.15: Two Fluid Results, Case 1: Heavy Species Temperature

walls were lost at the channel exit in Case 1. Although the electrodes will be heated by the diffusing particles, electrode temperature is not included in the model. However, as shown in Table 5.3 for Case 4, ambipolar loss absorbs a substantial fraction of the dissipation, so that there will be a great deal of electrode heating.

5.4 Viscosity

Recent work by Kilfoyle [6] and Kuriki [7] both show gas temperatures which equal and even exceed the electron temperatures. Kilfoyle finds T_g ranging from 1eV up to 7eV, or up to 80,000K. Kuriki finds heavy particle temperatures of up to 70,000K. As shown in Figure 5.15, the inviscid model predicts gas temperatures of only 5000K. Some additional source, not modeled in Section 5.2 must be adding energy to the heavy species. Heimerdinger et al. [4] and Kilfoyle [6] propose viscous dissipation as this source. Therefore, the model of Section 5.2 was adapted to include viscosity. As described in Section 2.4 a viscous dissipation term is added to the source terms in the overall momentum equation and the heavy species temperature equation. The results for this model are labeled as Case 3 in Figures 5.3 - 5.12. The electric field, viscosity coefficient, and velocity are shown in Figures 5.17, 5.18, and 5.19. As can be seen in these figures, the heavy species temperature increases to the levels found experimentally. This would seem to justify the hypothesis that viscous effects could cause high heavy species temperatures. The higher temperature leads to higher pressure throughout the channel. Also, the flow now

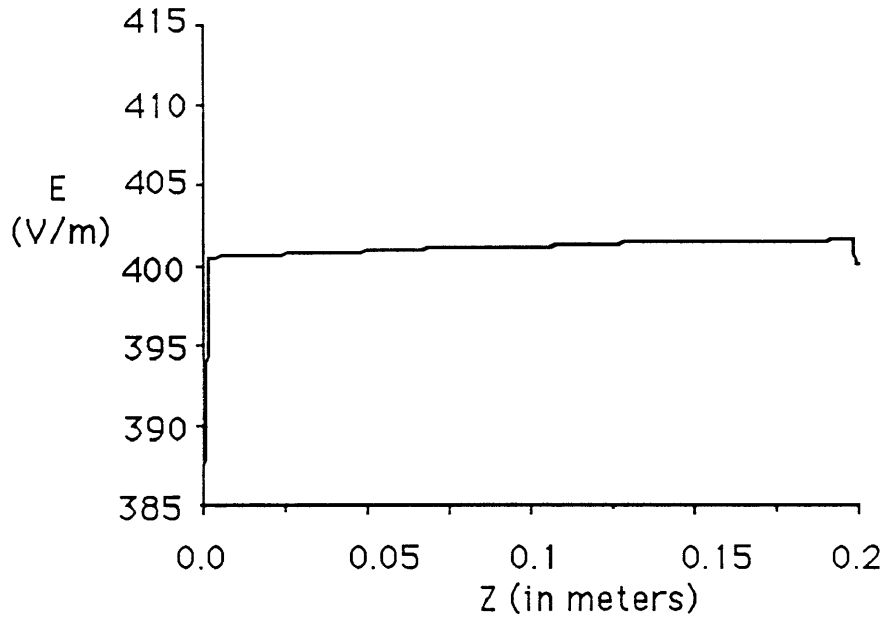

Figure 5.16: Two Fluid Results, Case 2: Electric Field

seems to be frictionally choked, so that the velocity levels off toward the beginning of the channel, and does not increase to the levels found in Section 5.2. The electric field has decreased from 401 V/m to 258 V/m, but the thrust and the efficiency have both dropped considerably, as shown in Table 8.1.

The variation of the viscosity through the channel, as shown in Figure 5.18, is also of interest. In the first part of the channel, the viscosity increases due to the increasing temperature, which leads to smaller neutral-neutral collison cross sections, and a higher viscosity. However, as the ionization fraction increases, the neutral viscosity become less important, and the viscosity is mostly due to the ions. As this is smaller than the neutral viscosity, the overall viscosity decreases with increasing ionization fraction. The viscosity begins to drop with the ionization fraction as low as 0.1. Presumably at higher currents, where the average ionization would be greater, the viscosity would start to increase again, due to the smaller cross-section in the ion-dominated regime.

Heimerdinger [3] also included viscosity, but assumed thermal equilibrium. He also computed the ionization fraction by balancing recombination with local ionization. His results show an ionization fraction which varies almost linearly with z. This is in part due to the large variation in the overall temperature which is used to compute the ionization. By separating the electron and heavy species temperatures, this research finds a lower ionization fraction in the bulk of the channel with the ionization fraction increasing sharply

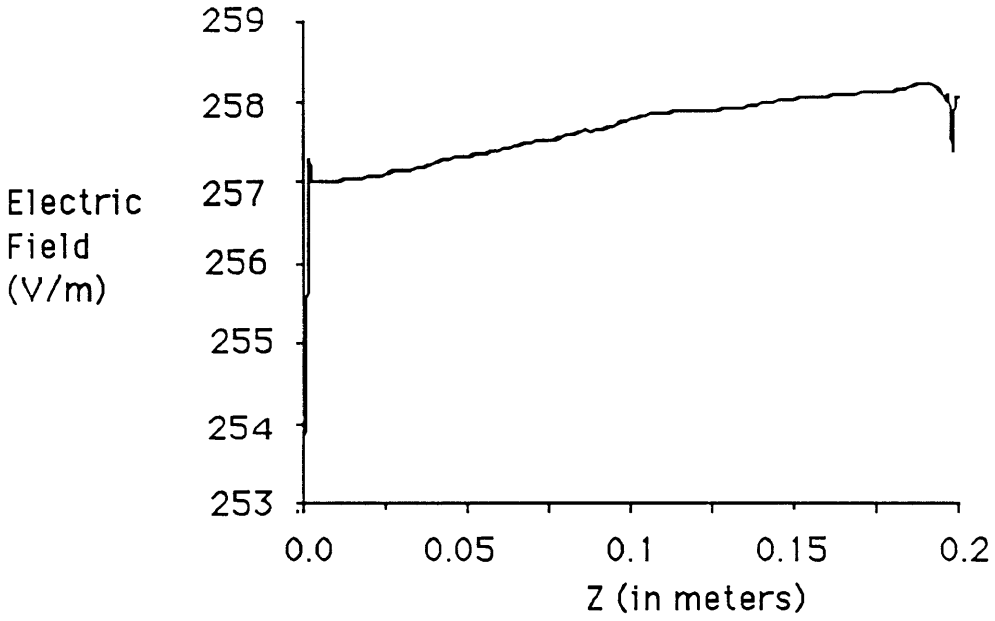

Figure 5.17: Two Fluid Results, Case 3: Electric Field

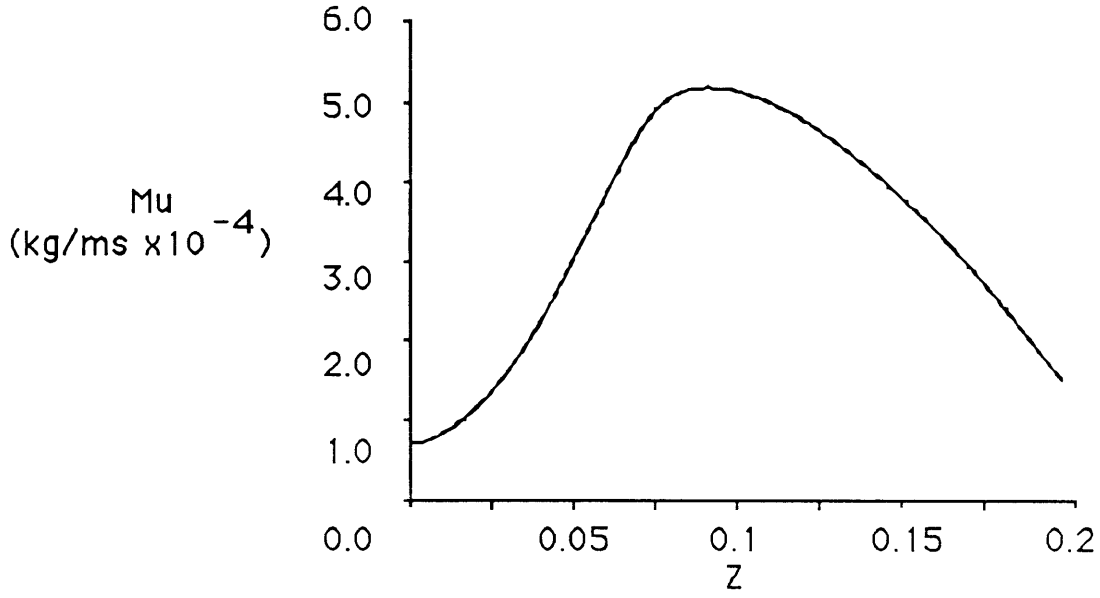

Figure 5.18: Two Fluid Results, Case 3: Viscosity Coefficient

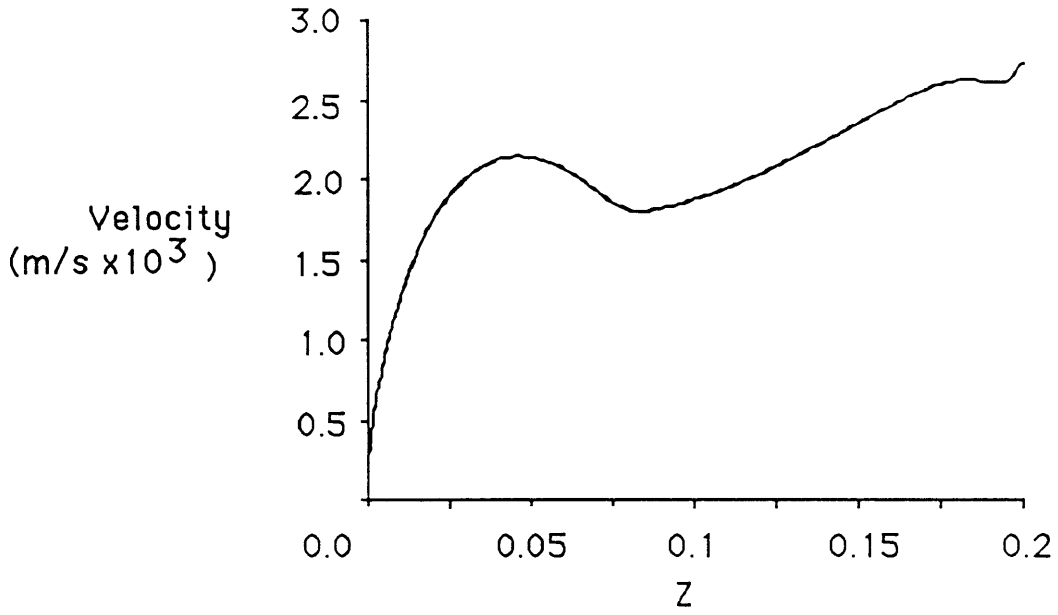

Figure 5.19: Two Fluid Results, Case 3: Velocity

at the exit. The variation of the viscosity coefficient and the velocity distribution are also quite different than in Heimerdinger.

5.5 Heat Conduction Results

One other process which was added to the model was electron heat conduction. This process was added to allow results to be obtained for higher overall currents. The need for heat conduction is explained in more detail in Chapter 6. The results for this case are labeled Case 4 in Figures 5.3 - 5.12. The electric field and heat conduction coefficient are shown in Figures 5.20 and 5.21 respectively. As can be seen in these figures, the results are quite similar to those of Case 3, although there are some differences. These differences are mainly due to the changed inlet boundary condition. As described in section 2.7.1, when heat conduction is present the last boundary condition is constant electron temperature at the inlet instead of one-sided differencing of the density. This boundary condition eliminates the sudden rise in electron temperature at the inlet, but introduces a sudden rise in the velocity and gas temperature and a sudden drop in the pressure and density. The higher inlet electron temperature also leads to a higher ionization fraction in most of the channel. The thrust and efficiency for this case are again shown in Table 8.1.

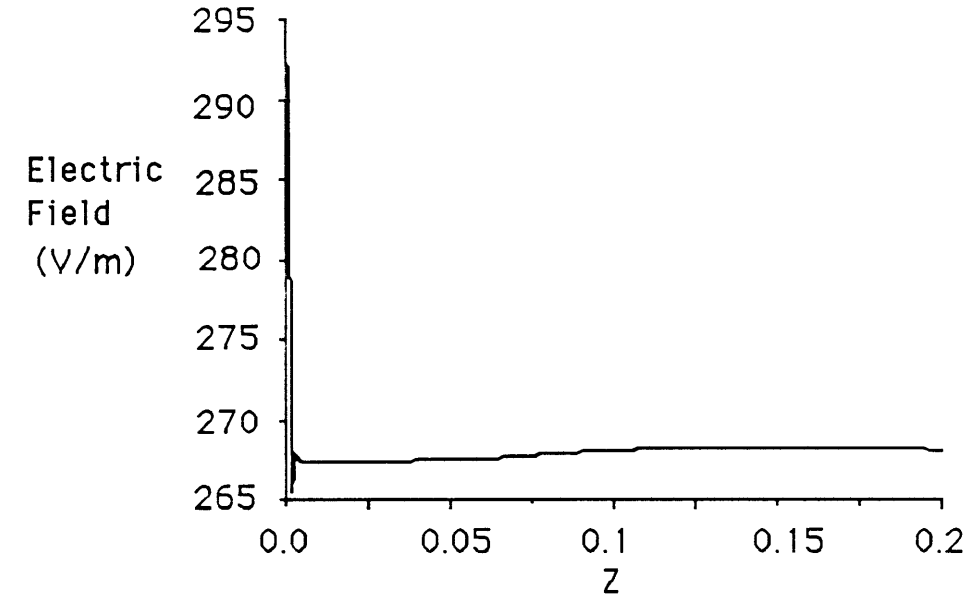

Figure 5.20: Two Fluid Results, Case 4: Electric Field

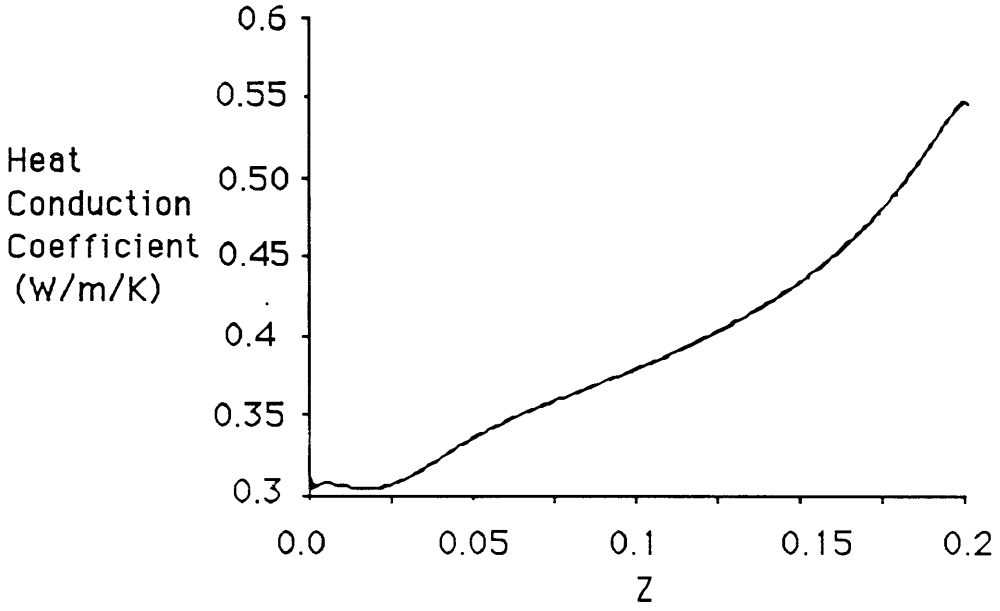

Figure 5.21: Two Fluid Results, Case 4: Heat Conduction Coefficient

Z(cm)	ionization	recombination	ambipolar diffusion
0.5	1.11	0.26	0.91
2.5	0.68	0.09	0.80
4.5	1.08	0.08	0.78
6.5	1.71	0.10	0.85
8.5	2.25	0.12	1.01
10.5	2.83	0.16	1.22
12.5	3.56	0.20	1.50
14.5	4.58	0.25	1.86
16.5	6.30	0.34	2.37
18.5	9.93	0.56	3.17

Table 5.2: Magnitude of Terms in the Ionization Fraction Equation

5.6 Relative Importance of Effects

In steady state, the ionization fraction equation becomes

$$\frac{\partial \alpha}{\partial z} = \frac{A}{\dot{m}} m_i R n_e S n_n - \frac{A}{\dot{m}} m_i R n_e^3 - \frac{A}{\dot{m}} m_i \frac{12 D_a n_e}{H^2} \tag{5.1}$$

For Case 4, the complete model, the magnitude of each of these effects at various locations in the channel is given in Table 5.2. It is seen that recombination is a relatively weak effect. At the beginning of the channel, ambipolar diffusion and ionization are almost equal. However, as the electron temperature increases, ionization becomes almost twice as large as ambipolar diffusion. The electron energy equation can also be broken down in this way. Again, in steady state,

$$\frac{E_i}{k}\frac{\partial \alpha}{\partial z} + \frac{3}{2} T_e \frac{\partial \alpha}{\partial z} + \frac{3}{2}\alpha \frac{\partial T_e}{\partial z} - \frac{\alpha T_e}{\partial} z \frac{\partial \rho}{\partial z} =$$

$$\frac{m_i}{k\rho U}\frac{J^2}{\sigma} - \frac{m_i}{k\rho U} E_l - \frac{m_i}{k\rho U}\frac{\partial}{\partial z}(K_e \frac{\partial T_e}{\partial z}) - \frac{m_i}{k\rho U} E_i 12 D_a \frac{n_e}{H^2}$$

In words, Ionization Energy + Temperature Energy + Electron Heating - Pressure Work = Dissipation - Collisional Transfer - Heat Conduction - Ambipolar Loss. The magnitude of each of these terms is given in Table 5.3. For the most part, dissipation is balanced by ionization energy and ambipolar loss, although collisional energy transfer is also a significant term, particularly near the inlet. Notice also that near the exit the ions are actually significantly heating the electrons. Heat conduction and electron heating play a small role, while pressure work is negligible.

Z(cm)	Ionization Energy	Temper. Energy	Electron Heating	Pressure Work	Dissi-pation	Collisional Transfer	Heat Cond.	Ambipolar Loss
0.5	0.59	0.05	0.03	-0.21	3.66	1.37	-0.37	1.67
2.5	-0.32	-0.03	0.02	-0.02	1.60	0.52	-0.16	1.46
4.5	0.46	0.04	0.03	0.01	2.12	0.22	-0.26	1.41
6.5	1.40	0.12	0.02	-0.01	3.02	-0.09	-0.16	1.56
8.5	2.05	0.18	0.02	-0.02	3.64	-0.48	-0.15	1.84
10.5	2.65	0.24	0.02	-0.03	4.27	-0.96	-0.17	2.24
12.5	3.39	0.31	0.03	-0.05	5.11	-1.47	-0.21	2.75
14.5	4.53	0.42	0.05	-0.07	6.53	-2.0	-0.28	3.42
16.5	6.65	0.64	0.08	-0.07	9.21	-2.56	-0.39	4.34
18.5	11.68	1.16	0.13	0.0	15.04	-3.40	-0.51	5.81

Table 5.3: Magnitude of Terms in the Electron Energy Equation, $\times 10^{-5}$

Chapter 6

Effects of Variation of Total Current

The addition of viscosity to the two fluid model produced frictional choking of the fluid, as described in Section 5.4. It was desired to determine if higher total currents would break through this thermal choking by producing higher ionization fraction in the bulk of the channel, and, therefore, lowered viscosity. It was also desired to see if the ionization instability described by Heimerdinger [4] could be simulated numerically. The results for three inlet magnetic fields, 0.1, 0.15, and 0.2T, using the complete model with ambipolar diffusion, viscosity and heat conduction, are shown in Figures 6.1 - 6.12. The electric fields for the three case are shown in Figures 5.20, 6.13, and 6.14.

As can be seen in Figure 6.5, the Mach number in the 0.15T case remains quite close to 1, after a jump at the inlet, although it does increase slightly. Unlike the 0.1 T case however, the velocity continues to rise throughout the channel, and begins to rise sharply at the exit, where the current is concentrated. The thrust and the efficiency, as given in Table 8.1, have both increased dramatically. The viscosity coefficient, as shown in Figure 6.12, increases only slightly due to the increased magnetic field, even though the gas temperature has more than doubled. In fact, at the end of the channel, the viscosity coefficient is smaller in the 0.15T case than in the 0.1T case. This is due to the increased ionization throughout the channel, shown in Figure 6.1.

Another noticeable feature of these results is the rise in electron temperature at the exit for B_0 of 0.15 and 0.2. Before the addition of electron heat conduction to the model, this rise caused an instability at the exit for B_0 greater than 0.15. This instability mimics the physical ionization instability discussed by Heimerdinger [4]. However, in a physical thruster the current at the exit would only build up to a certain point, and then it would follow a path which would lead it outside of the channel and then back into the channel. This longer path would decrease the effective conductivity of the exit, and would eventually lead to a quenching of the current there. Since the total current in the channel is constant, the current which would no longer be flowing at the exit would

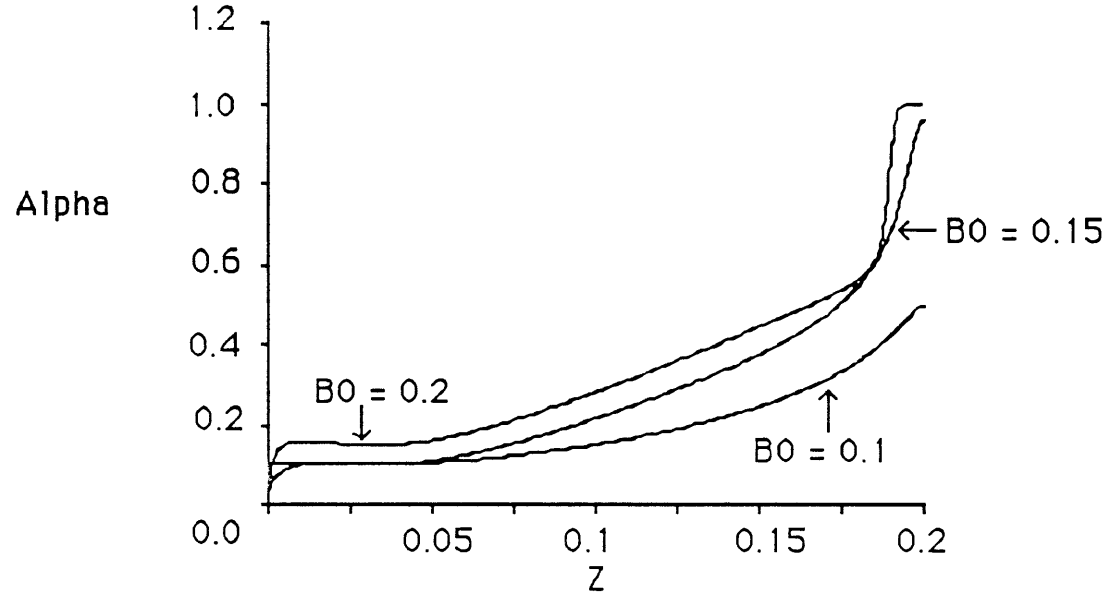

Figure 6.1: Varying Total Current:Ionization Fraction

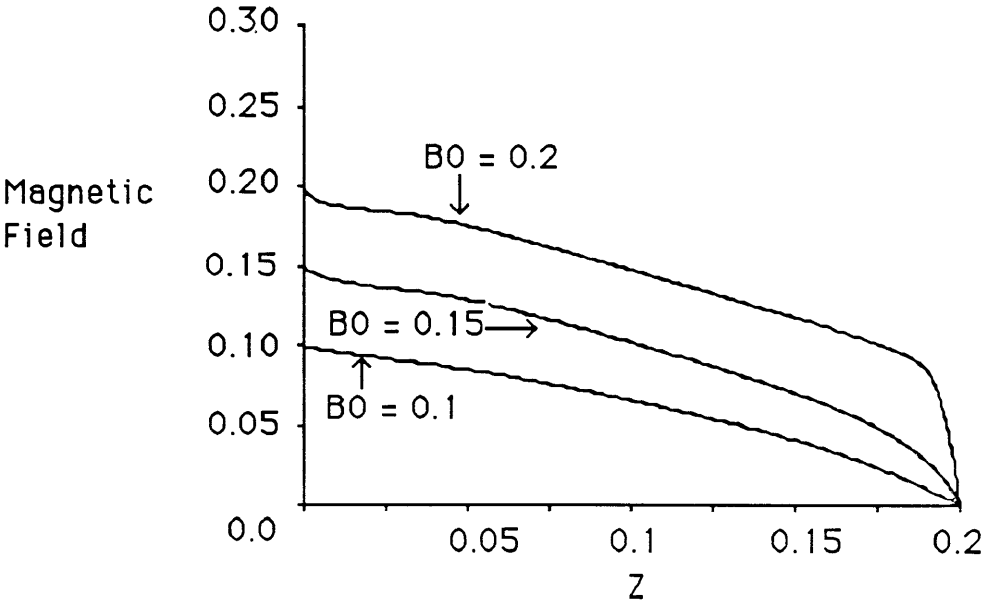

Figure 6.2: Varying Total Current:Magnetic Field

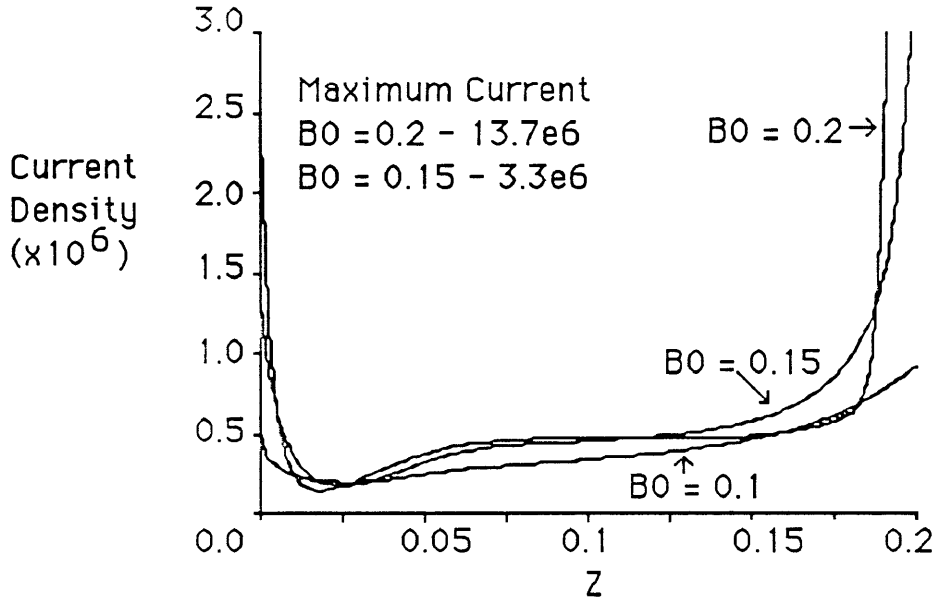

Figure 6.3: Varying Total Current:Current Density

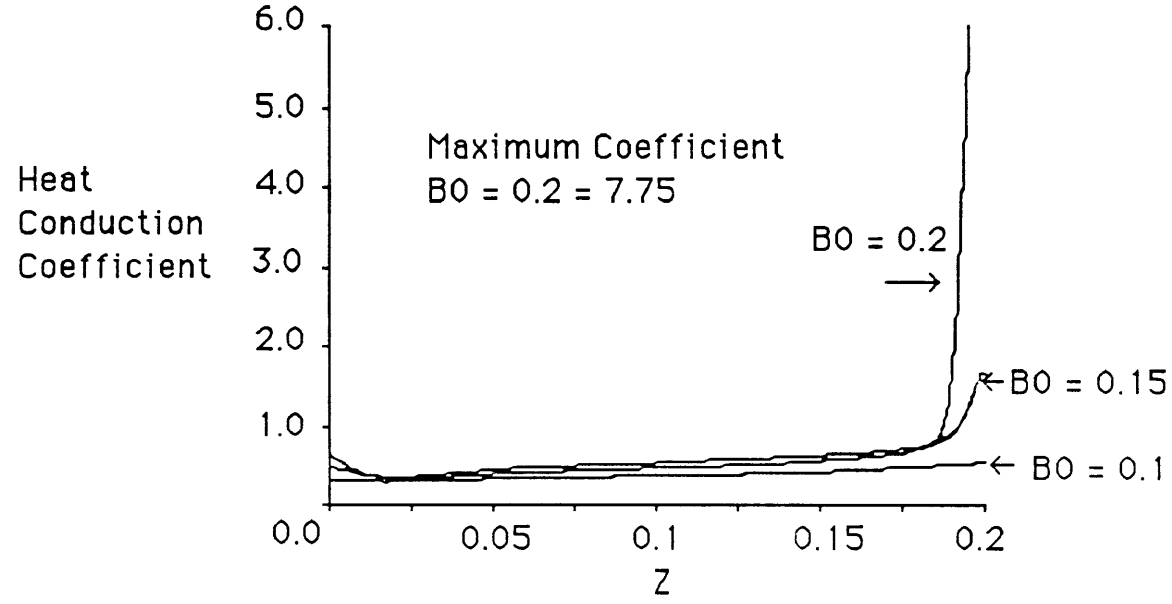

Figure 6.4: Varying Total Current:Heat Conduction Coefficient

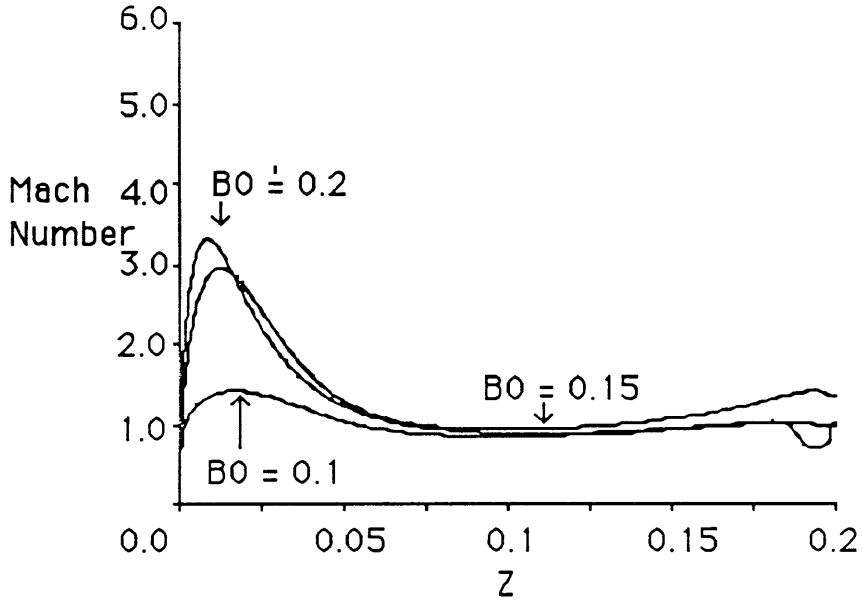

Figure 6.5: Varying Total Current:Mach Number

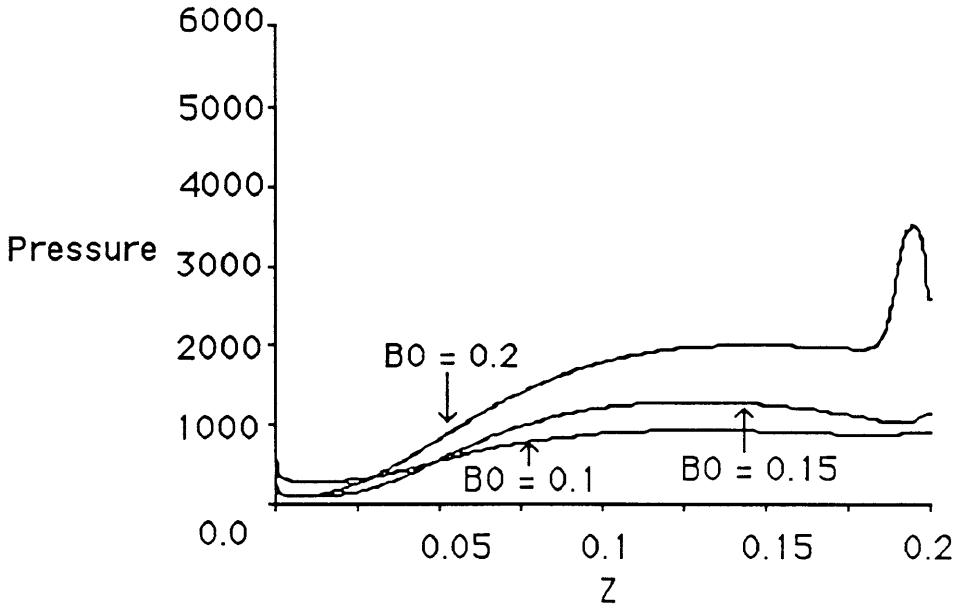

Figure 6.6: Varying Total Current:Pressure

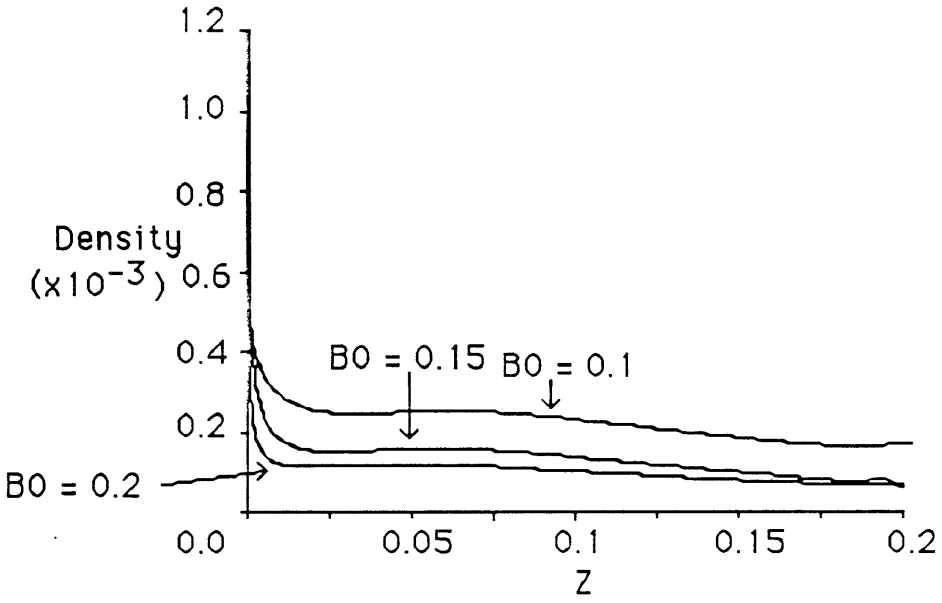

Figure 6.7: Varying Total Current:Density

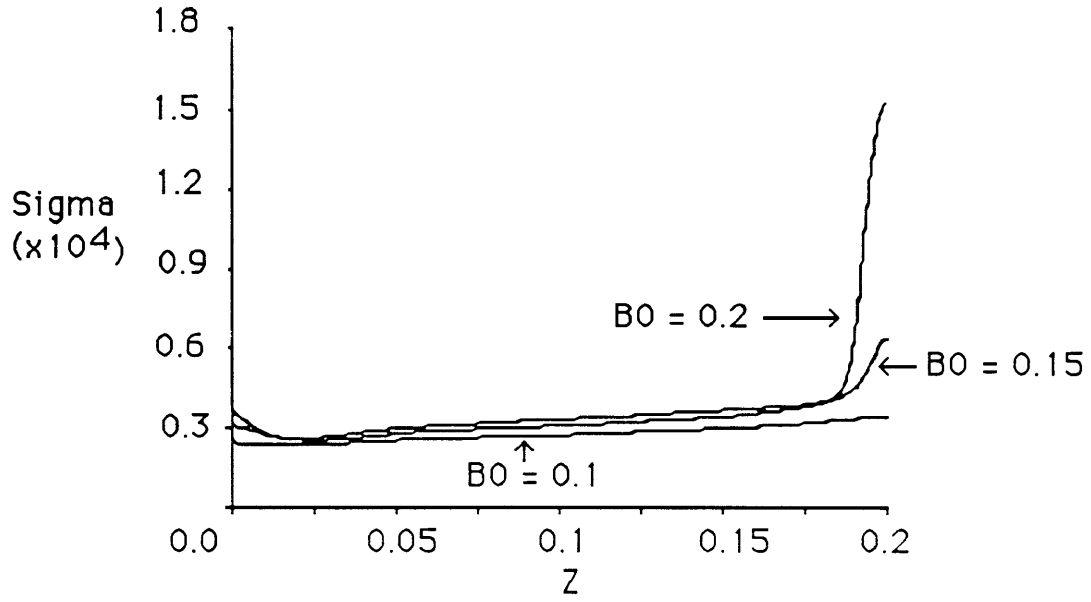

Figure 6.8: Varying Total Current:Conductivity

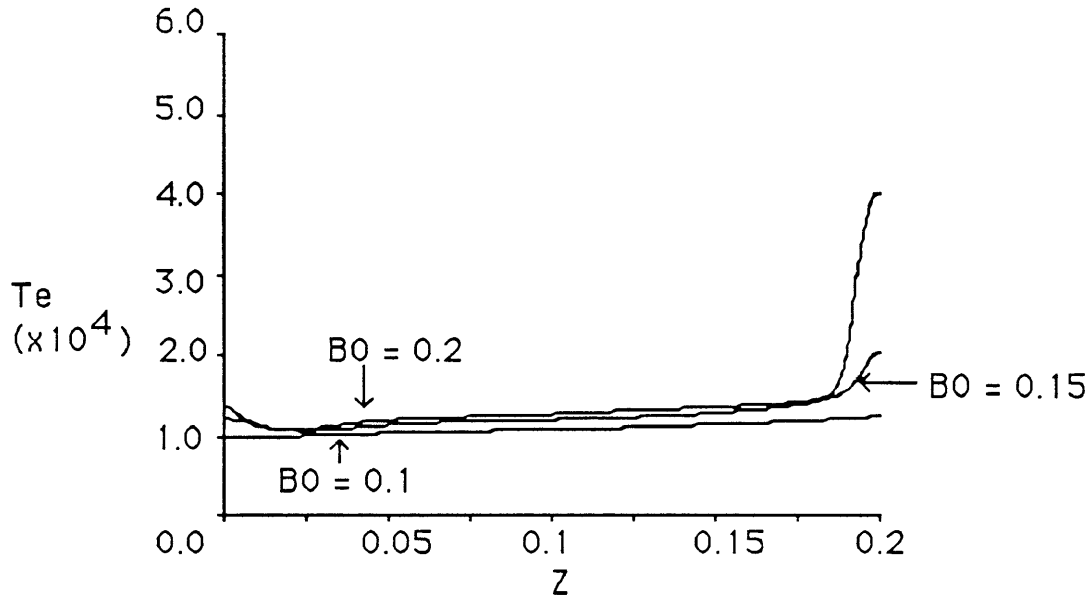

Figure 6.9: Varying Total Current:Electron Temperature

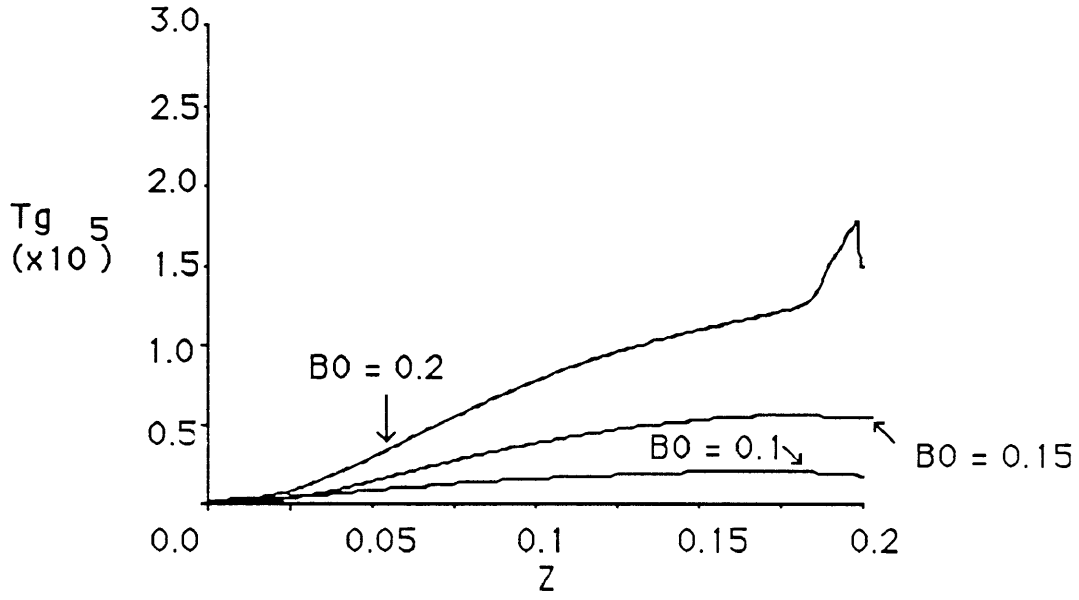

Figure 6.10: Varying Total Current:Gas Temperature

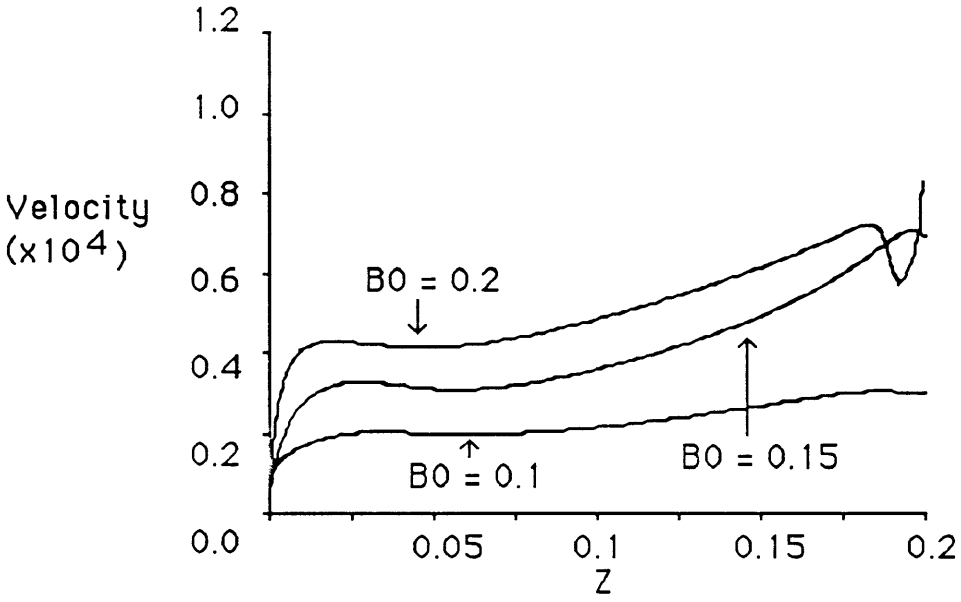

Figure 6.11: Varying Total Current:Velocity

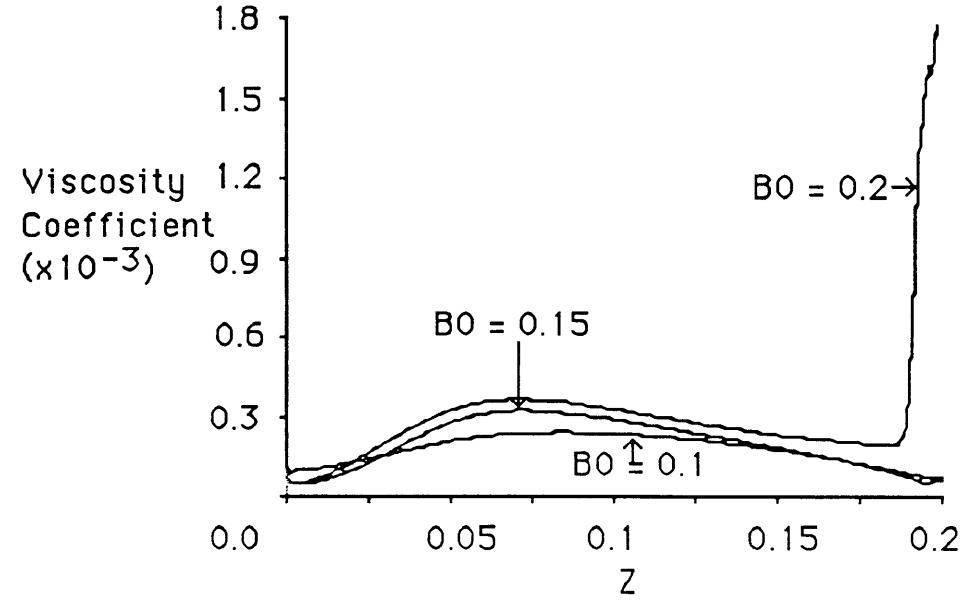

Figure 6.12: Varying Total Current:Viscosity Coefficient

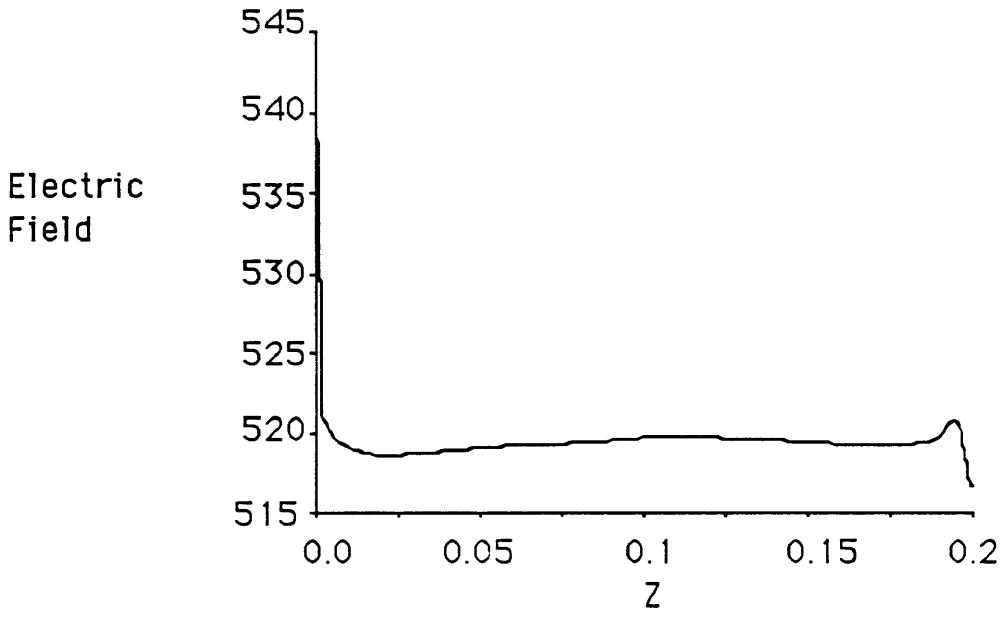

Figure 6.13: Electric Field, B_0=0.15T

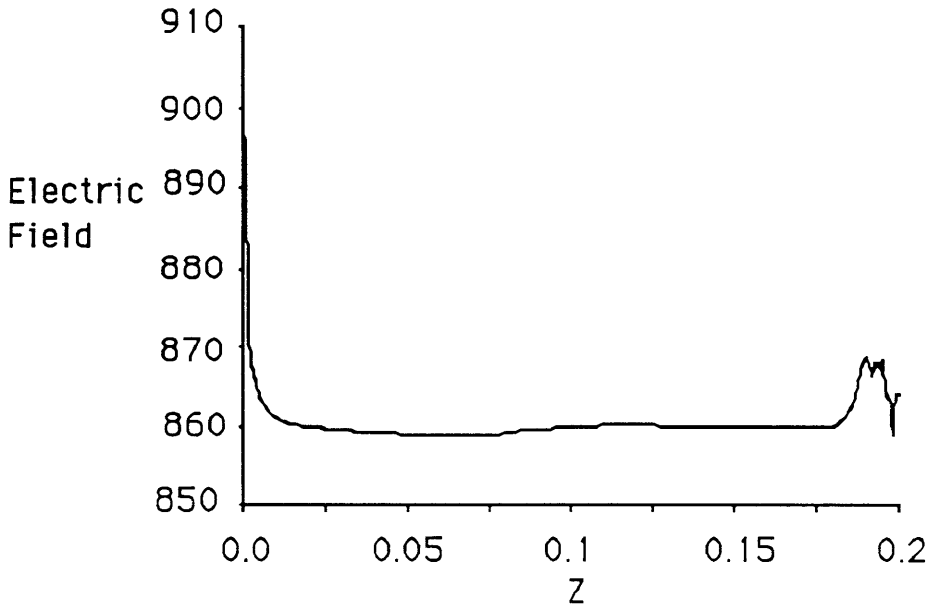

Figure 6.14: Electric Field, B_0=0.2T

be forced elsewhere in the channel. The current spike created would then be convected down the channel with the fluid. A periodic oscillation, with a period close to the flow time, would begin. However, because of the one dimensional nature of this model and the zero exit magnetic field condition, the current is not allowed to flow outside the exit, and current continues to build up at the exit. Therefore this instability is not a physical one. However, it does seem to be clear that some physical instability is occuring as the ionization fraction approaches unity. This instability seems to appear between B_0 = 0.15 and 0.2 Tesla, corresponding to currents of 119 to 159 $\frac{kAmp}{m \cdot depth}$. Heimerdinger and Martinez [5] observed this instability for currents of 127 $\frac{kAmp}{m \cdot depth}$ for their constant area channel. Reproducing the physical instability would require considerable care and insight in the simplified model used in this research.

The addition of electron heat conduction to the model alleviates the instability problem somewhat, allowing inlet magnetic fields of up to 0.2T. However, above 0.2T the number of time steps necessary for the electron heat conduction term becomes prohibitive, because of very high transient electron temperatures, and the numerical scheme does not seem to converge. This problem could be solved by finding a more appropriate initial condition, but one has not yet been found. Because of the non-physical nature of the instability, the validity of the numerical results for high inlet current, particulary near the exit of the channel, is questionable. The 0.2T results in particular are uncertain. As can be seen in Figure 6.14, the electric field for this case varies not just at the exit, but also within the channel itself. In addition, the exit massflow for this case does not come within the 1 % error criterion discussed in Section 4.1. This was true no matter how long the simulation was run for. Also, the simulation experiences very large transients, especially in electron temperature, in arriving at the results shown. These transients need to be investigated further.

It is also interesting to compare the effects of electron heat conduction in this two fluid model with the effects in Minakuchi's work [7] for a one fluid model. In the one fluid model, where electrons and heavy species are in thermal equilibrium, the addition of heat conduction spreads the exit temperature rise over the whole channel. In the two fluid model, where electron and heavy species temperature are almost decoupled, the effect of electron heat conduction is much smaller, and only spreads the electron temperature rise over a small area. This seems to indicate that the dissipation of the temperature rise over the whole channel is an artifact of the one fluid model.

Chapter 7

Effects of Area Variation

As described in Section 2.5, the quasi one dimensional equations can be used for channels with area variation. This chapter examines the flow in a converging-diverging, or fully flared, channel (FFC). Again, the method was tested for the one fluid model with area variation against the results of Martinez [10]. The results were almost identical to those given by Martinez. The interelectrode seperation for the channel is shown in Figure 7.1. The flow is compared to that in a constant area channel (CAC) in Figures 7.2 - 7.14. The potential is shown in Figure 7.15.

Heimerdinger [3] proposes area variation as a means of reducing inlet and exit current concentrations. This is seen to be the case, particularly at the exit. The thruster studied in this research has the same interelectrode seperation as that designed by Heimerdinger, but is almost twice as long. Also, the inlet current examined in this case is not the same as his design current. It is possible that for the same physical thruster as that chosen by Heimerdinger, this effect would be more pronounced.

As given in Table 8.1, there is a significant increase in performance for the variable area channel. This is in part due to a decrease in the effect of viscosity on the velocity, as the viscous source term in the momentum equation varies as $\frac{U}{H^2}$ Since both U and H have increased, the magnitude of this term has dropped. One other difference with the constant area channel is the higher electron temperature in the fully flared channel. This can be explained by examining Table 7.1 which gives the magnitude of the terms in the electron energy equation. Comparing this table to Table 5.3 points out a number of differences between the two channels. First, collisional energy transfer at the ends of the FFC is around 50% of its value at the ends of the CAC. This is because collisional energy transfer scales with density, which is smaller at the ends of the FFC, because of the increased area. Ambipolar loss is also smaller at the ends of the FFC, because of the increased interelectrode distance. Both of these lead to higher electron temperature. In the center of the channel, where both of these effects are of the same magnitude as in the CAC,

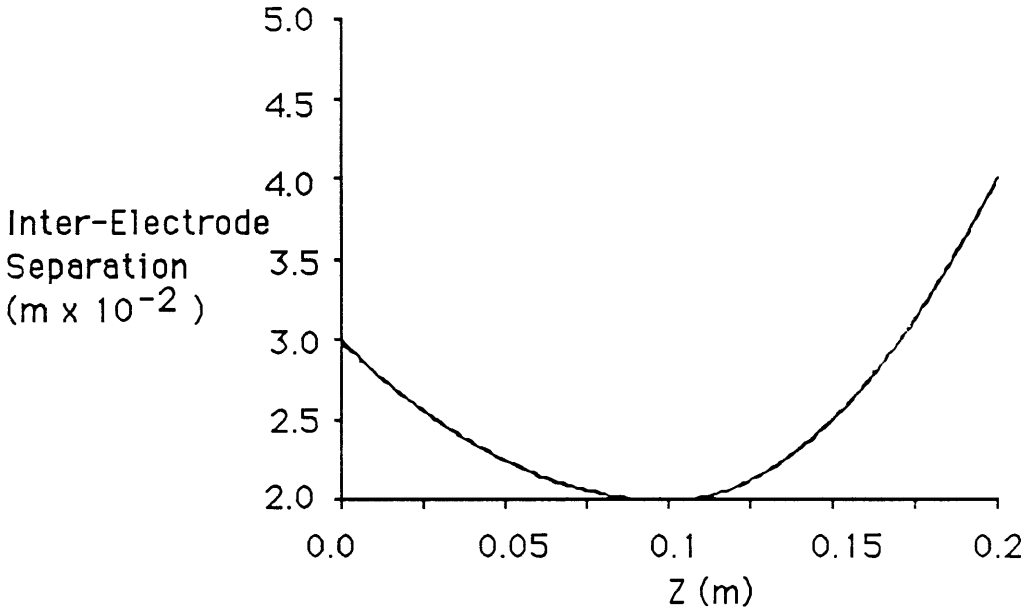

Figure 7.1: Inter-Electrode Separation of Fully Flared Channel

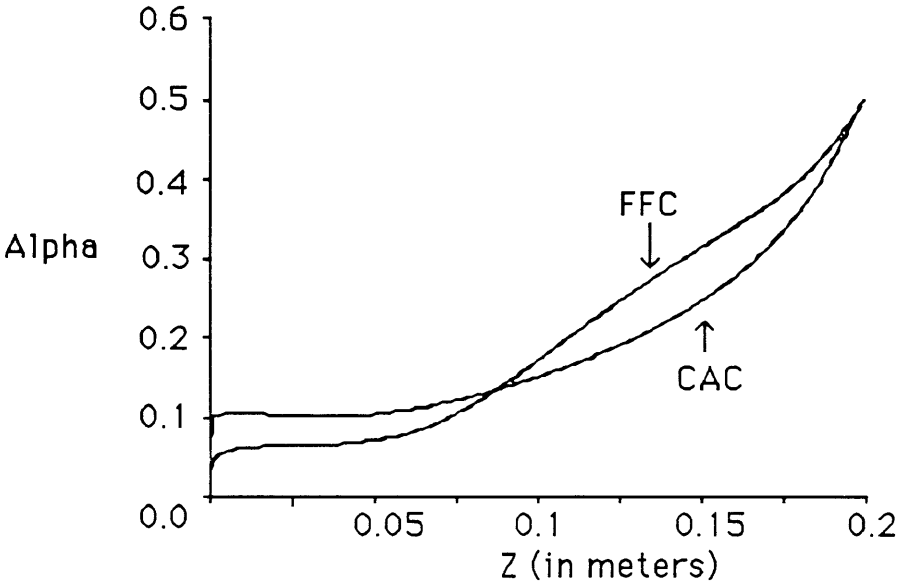

Figure 7.2: Fully Flared and Constant Area Channels: Ionization Fraction

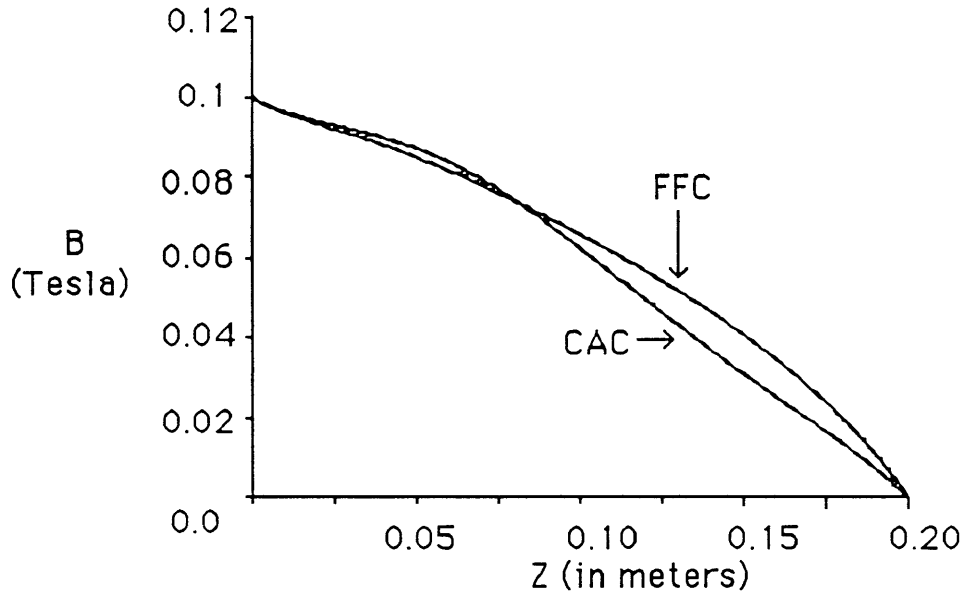

Figure 7.3: Fully Flared and Constant Area Channels: Magnetic Field Strength

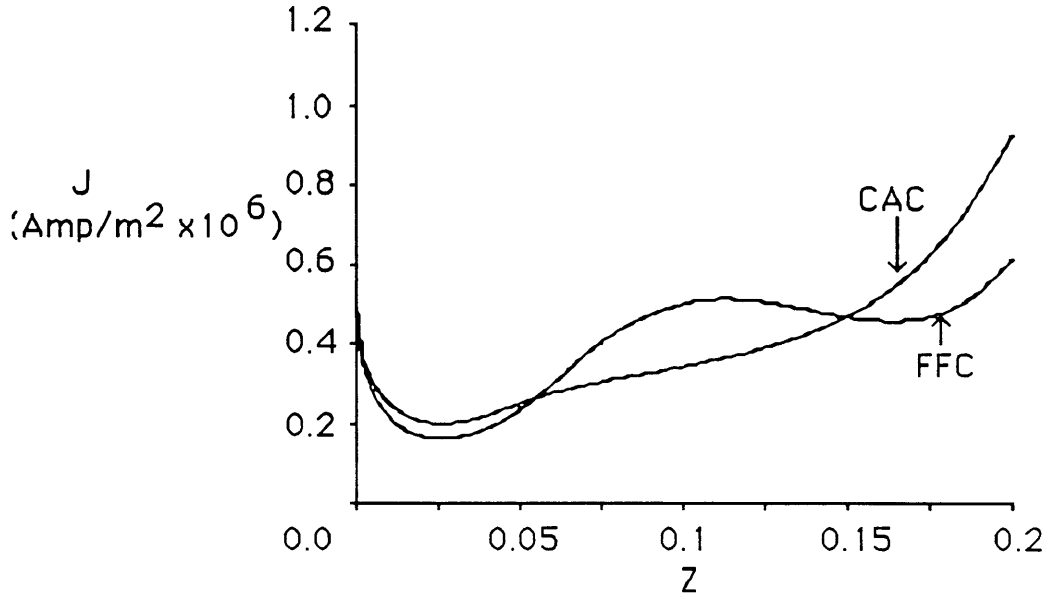

Figure 7.4: Fully Flared and Constant Area Channels: Current Density

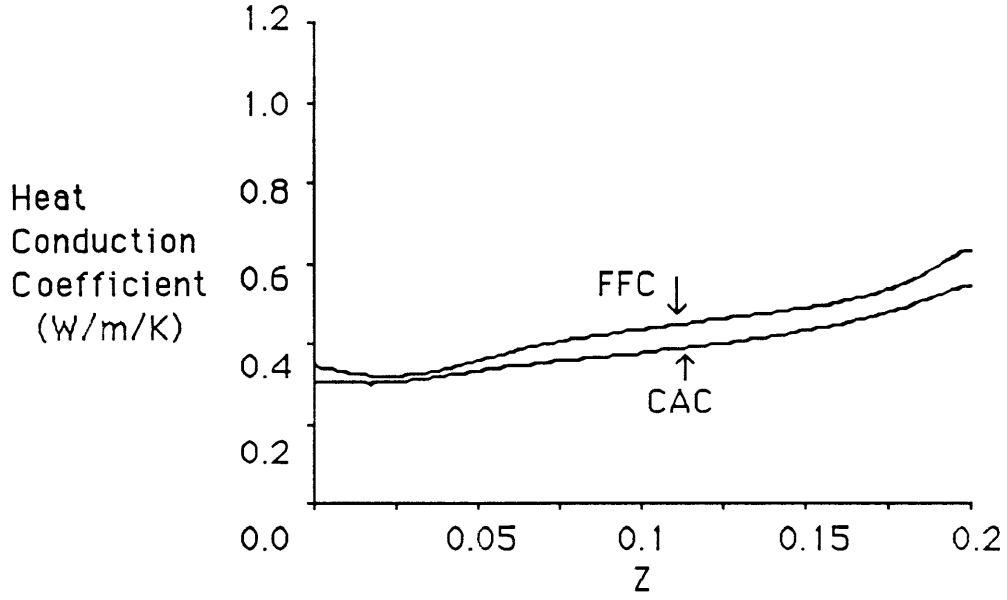

Figure 7.5: Fully Flared and Constant Area Channels: Heat Conduction Coefficient

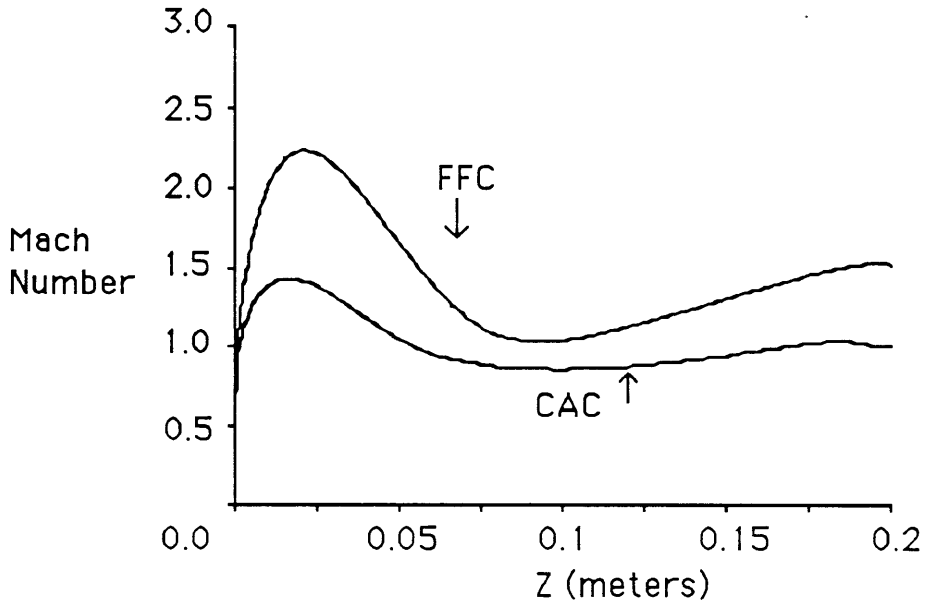

Figure 7.6: Fully Flared and Constant Area Channels: Mach Number

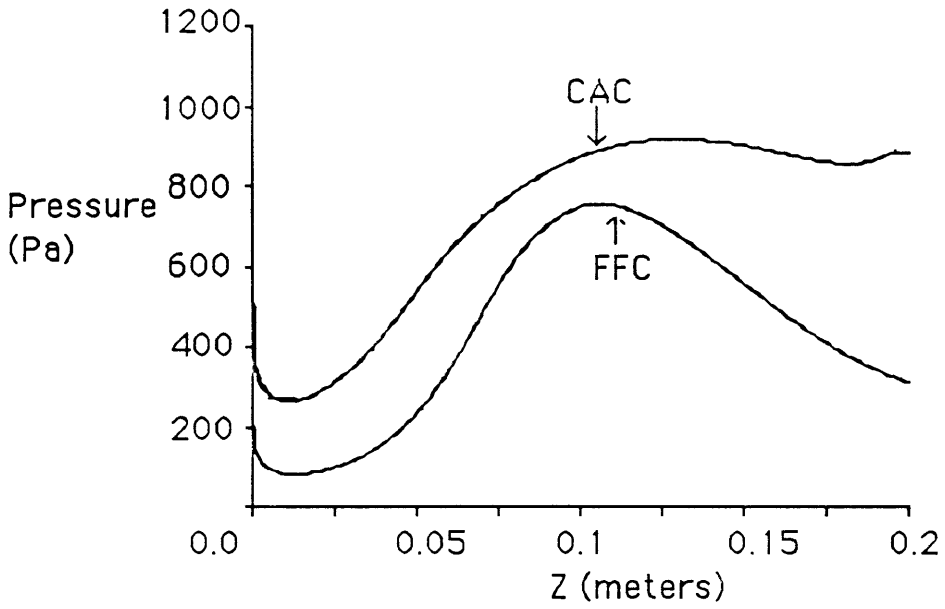

Figure 7.7: Fully Flared and Constant Area Channels: Pressure

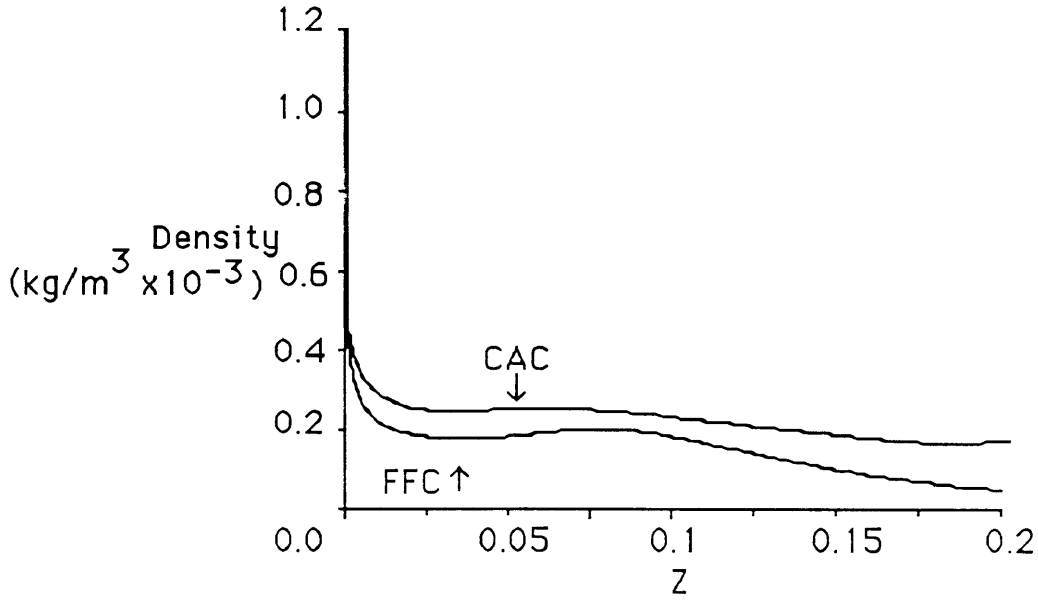

Figure 7.8: Fully Flared and Constant Area Channels: Density

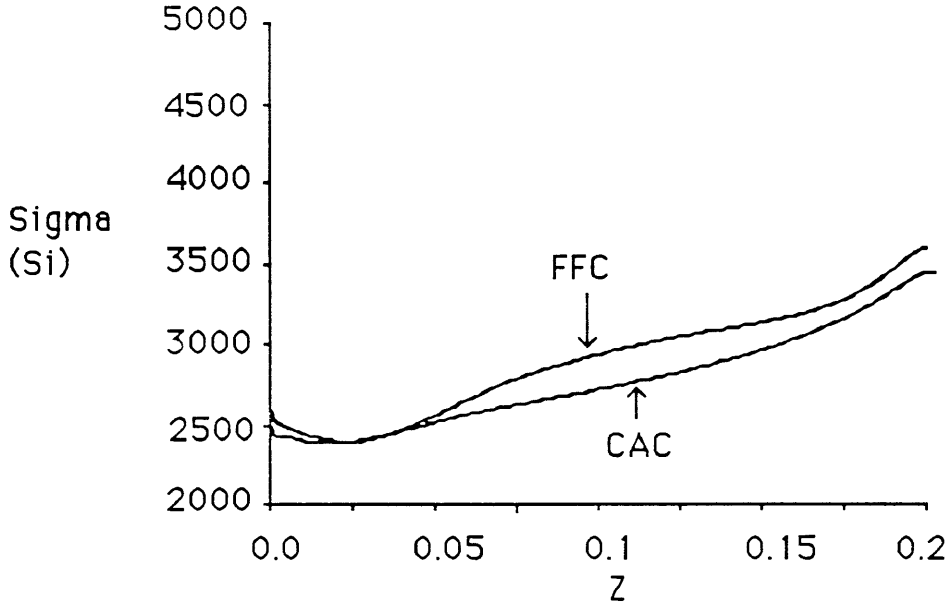

Figure 7.9: Fully Flared and Constant Area Channels: Conductivity

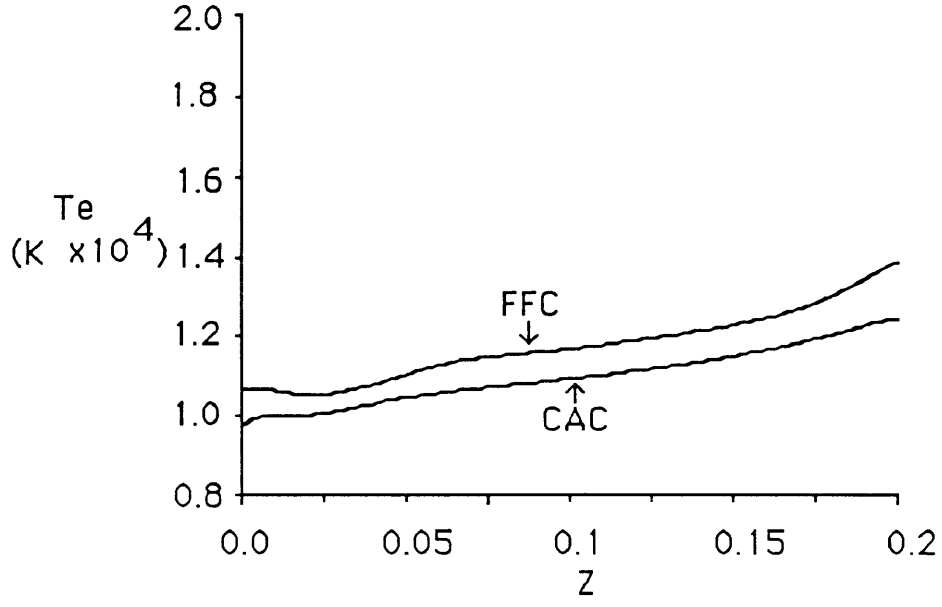

Figure 7.10: Fully Flared and Constant Area Channels: Electron Temperature

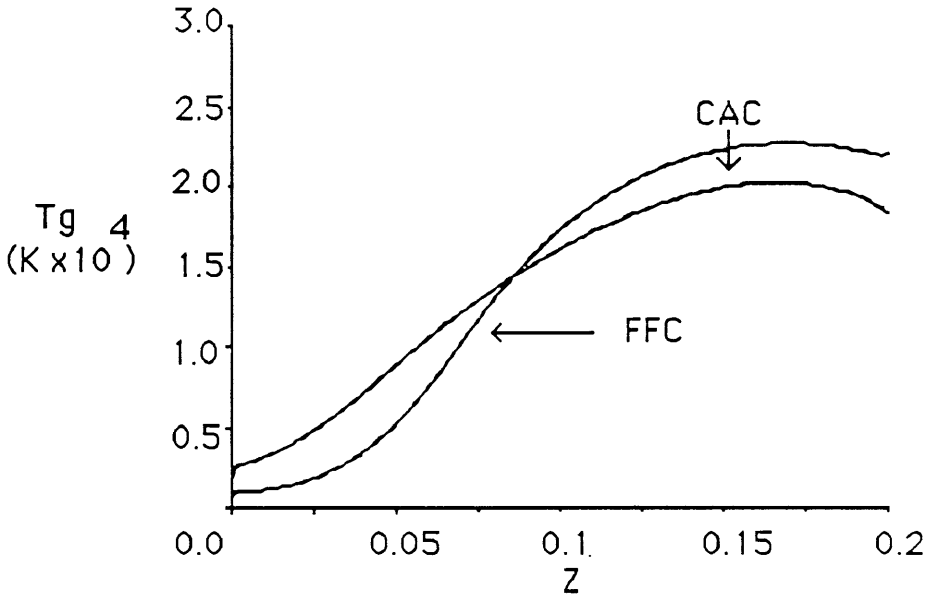

Figure 7.11: Fully Flared and Constant Area Channels: Gas Temperature

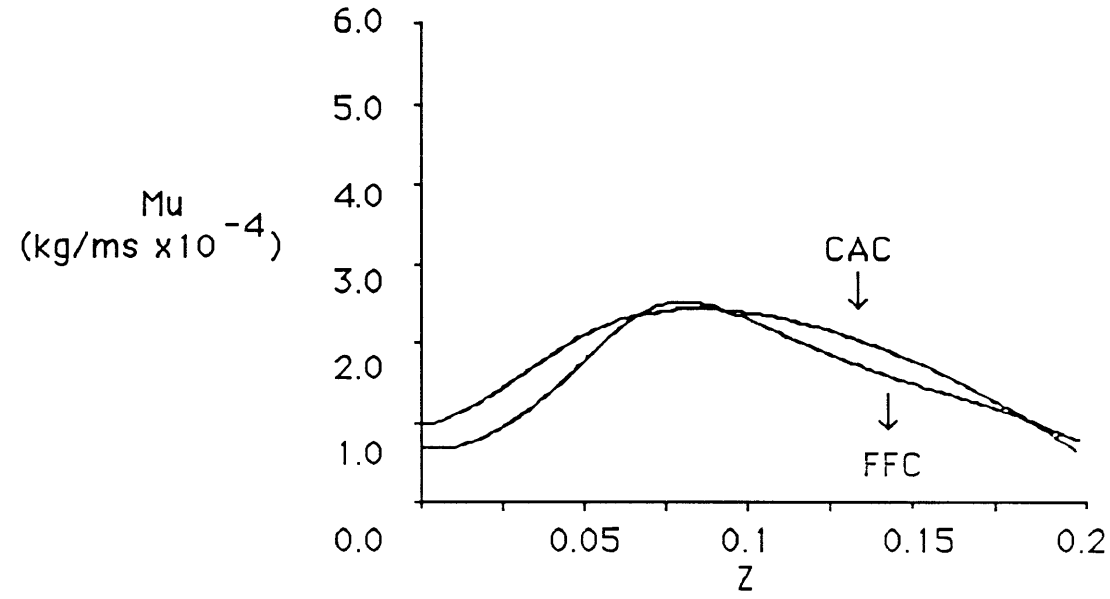

Figure 7.12: Fully Flared and Constant Area Channels: Viscosity Coefficient

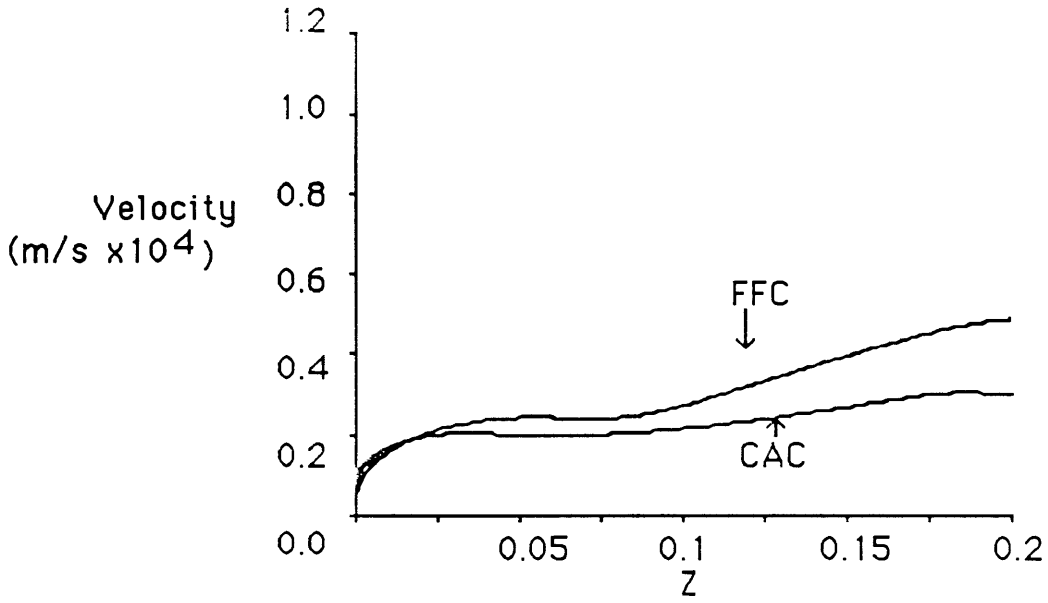

Figure 7.13: Fully Flared and Constant Area Channels: Velocity

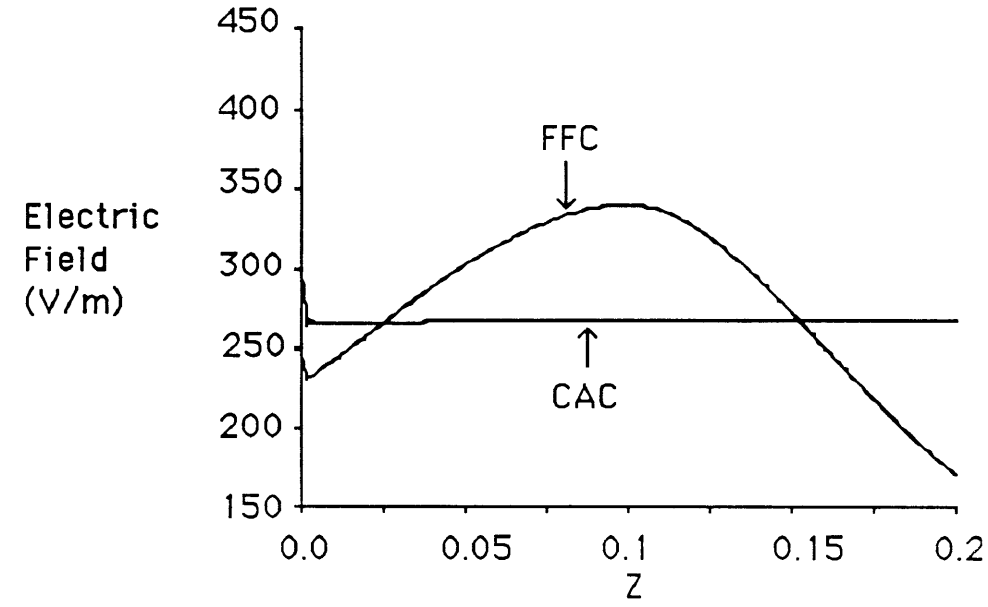

Figure 7.14: Fully Flared and Constant Area Channels: Electric Field

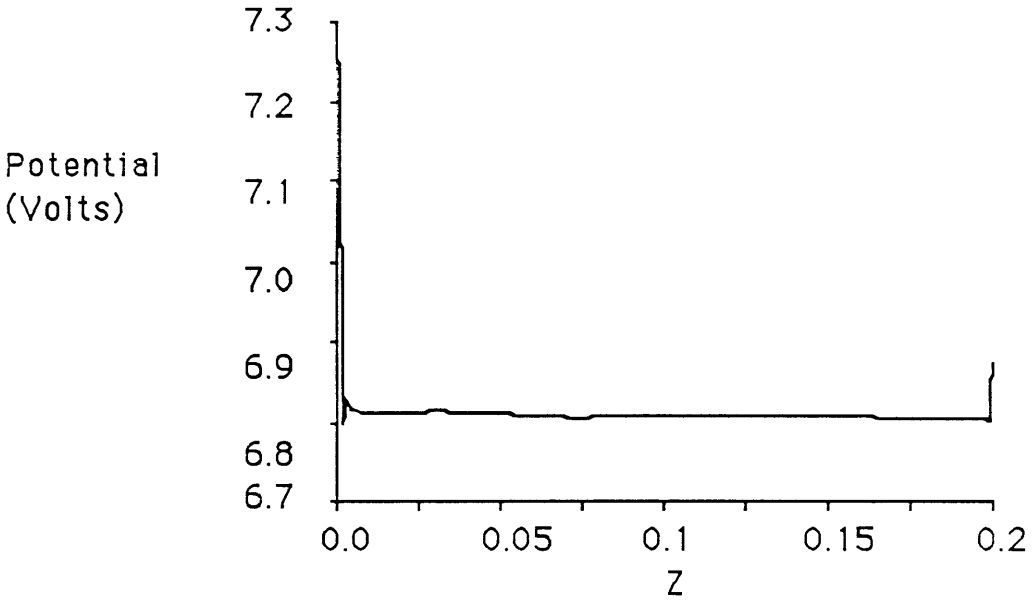

Figure 7.15: Potential for Fully Flared Channel

the increased throat dissipation of the FFC keeps the electron temperature higher than in the CAC. The lower collisonal energy transfer also makes the gas temperature lower at the beginning of the FFC. As velocity increases and viscosity becomes important in raising the gas temperature, the higher velocity in the FFC makes for higher gas temperature. The breakdown of terms for the ionization fraction is given in Table 7.2. Ionization is higher than in the CAC at the throat, where dissipation is higher, and lower at the exit, where dissipation is lower than in the CAC.

Z(cm)	Ionization Energy	Temper. Energy	Electron Heating	Pressure Work	Dissi-pation	Collisional Transfer	Heat Cond.	Ambipolar Loss
0.5	2.48	0.22	0.0	-0.17	4.32	0.50	-0.09	0.94
2.5	0.19	0.02	0.01	-0.02	1.34	0.23	-0.09	0.96
4.5	0.78	0.07	0.03	0.01	1.90	0.16	-0.46	0.93
6.5	2.70	0.25	0.02	0.02	4.16	0.10	-0.33	1.17
8.5	4.82	0.46	0.01	-0.03	6.97	-0.22	-0.14	1.83
10.5	5.56	0.53	0.03	-0.10	8.31	-0.83	-0.22	2.74
12.5	5.24	0.51	0.04	-0.18	8.43	-1.29	-0.28	3.48
14.5	4.75	0.48	0.07	-0.25	8.24	-1.43	-0.39	3.81
16.5	5.04	0.52	0.12	-0.32	8.81	-1.31	-0.77	3.84
18.5	7.83	0.85	0.28	-0.36	12.15	-1.10	-1.97	3.83

Table 7.1: Magnitude of Terms in the Electron Energy Equation, $\times 10^{-5}$

Z(cm)	ionization	recombination	ambipolar diffusion
0.5	1.66	0.02	0.51
2.5	0.62	0.01	0.52
4.5	0.92	0.01	0.51
6.5	2.09	0.02	0.64
8.5	3.69	0.05	1.00
10.5	4.65	0.09	1.49
12.5	4.90	0.10	1.90
14.5	4.79	0.09	2.08
16.5	4.91	0.06	2.10
18.5	6.34	0.04	3.09

Table 7.2: Magnitude of Terms in the Ionization Fraction Equation

Chapter 8

Conclusions

8.1 Performance

The thrust and efficiency for the various cases are shown in Table 8.1. There are a number of loss mechanisms that prevent the thruster from being 100% efficient. One reason for the decreased efficiency is the frozen flow losses. Since the residence time of the fluid in the channel is short, the composition of the fluid is not the equilibrium composition. Therefore, some of the energy used to ionize the neutral fluid is not recovered. Ambipolar diffusion, although it changes where losses occur, does not seem to change the amount of loss. However, adding viscosity to the model does cause a large drop in efficiency. At the low inlet magnetic field, heat conduction does not affect the efficiency significantly. Raising the total current improves efficiency, as does channel area variation.

8.2 Need for a Two Fluid Model

The results presented here are some of the first this author has seen for two fluid MPD flows. As such, it is important to compare them to one fluid models, to help evaluate the need for a two fluid model. The performance predictions for the one fluid model and two fluid model for a similar case, (one fluid -R_{mag}=4.9258, two fluid -B_0 = 0.1, no viscosity, no heat conduction) differ by only 7%. More significant however is the effect of viscosity. Adding viscosity to the simulation cut the performance of the thruster in half. The viscous coefficient used in this model depends on separate species temperatures and a finite ionization fraction. The way this coefficient varies in the channel as the ionization and gas temperature increase has substantial effects on the flow. It would be hard to model this viscosity in a similar manner in a one fluid model. Therefore, two fluid simulations would seem to be important in predicting the performance of MPD thrusters.

Case	R_{mag} or B_0	ambipolar diffusion	viscosity	heat conduction	channel	E_t V/m	$\tilde{T}$ N/m^2	η
1-fluid	20	no	no	no	CAC	345	4370	0.69
1-fluid	4.9258	no	no	no	CAC	433	4630	0.62
2-fluid	0.1	no	no	no	CAC	399	4256	0.57
2-fluid	0.1	yes	no	no	CAC	401	4180	0.55
2-fluid	0.1	yes	yes	no	CAC	258	2100	0.21
2-fluid	0.1	yes	yes	yes	CAC	287	2300	0.23
2-fluid	0.15	yes	yes	yes	CAC	519	4550	0.33
2-fluid	0.2	yes	yes	yes	CAC	860	6980	0.33
2-fluid	0.1	yes	yes	yes	FFC	340	3053	0.34

Table 8.1: Thrust and Efficiency for All Cases

8.3 Results

This research had a number of goals, as described in the Introduction. The first was to develop a numerical method with which to analyze a two fluid model. That goal has been achieved. The method developed has proven to be very versatile, and should become a useful tool in thruster analysis. Also, the method has been tested against previous one fluid work and has been shown to be accurate. A second goal was to determine the effect of viscosity on the thruster fluid flow. It has been seen that viscosity raises the gas temperature to levels found experimentally. The research was not as successful in finding the ionization instability, although a hint of that instability is found at high currents. It is also shown that area variation can increase efficiency by a significant amount.

8.4 Further Work

This simulation, even within the restricted model used, noticeably falls short in one area, that of increasing the total current and finding the ionization instability. Even with the 0.2T results shown, the exit current buildup is problematic. Accurately modeling the ionization instability would require allowing this current to "exit" from the channel. Also, as discussed earlier, the severe transients associated with this case need to be investigated. All in all, work needs to be done to allow for reliable simulation of higher total currents.

Once satisfactory results are obtained for higher currents, the next area of work is the expansion of the model. Viscosity and diffusion are both multi-dimensional effects. They

have only been modeled crudely in this research, and yet their effects on performance are tremendous. The Hall Effect, again multi-dimensional in nature, has been completely ignored in this model. Two dimensional axisymmetric codes which include viscosity and diffusion are urgently needed. This research represents only one step towards the understanding of MPD flows, and much more research remains to be done.

Bibliography

[1] Dale A. Anderson, J.C. Tannehill and R.H. Pletcher, *Computational Fluid Mechanics and Heat Transfer*, Hemisphere Publishing Corporation, New York

[2] J.M.G. Chanty and M. Martinez-Sanchez, "Two-Dimensional Numerical Simulation of MPD Flows", AIAA-87-1090, AIAA/DGLR/JSASS 19th International Electric Propulsion Conference, Colorado, May 1987

[3] D.J. Heimerdinger, "Fluid Mechanics in a Magnetoplasmadynamic Thruster", Doctoral Thesis, Massachusetts Institute of Technology, Jan. 1988

[4] D.J. Heimerdinger, D.B. Kilfoyle, and M. Martinez-Sanchez, "Experimental Characterization of Contoured Magnetoplasmadynamic Thrusters", AIAA-88-3205 AIAA/ASME/SAE/ASEE 24th Joint Propulsion Conference, Boston, July 1988

[5] D.J. Heimerdinger and M. Martinez-Sanchez, "Fluid Mechanics in a Magnetoplasmadynamic Thruster", IEPC-88-039, DGLR/AIAA/JSASS 20th International Electric Propulsion Conference, West Germany, Oct. 1988

[6] D.B. Kilfoyle, M. Martinez-Sanchez, D.J. Heimerdinger, and E.J. Sheppard, "Spectroscopic Investigation of the Exit Plane of an MPD Thruster", IEPC-88-027, DGLR/AIAA/JSASS 20th International Electric Propulsion Conference, West Germany, Oct. 1988

[7] Y. Kunii, "Multipole MPD Arcjet", AIAA-85-2055, AIAA/DGLR/JSASS 18th International Electric Propulsion Conference, Virginia, Sept. 1985

[8] K. Kuriki, Y. Kunii, and Y. Shimizu, "Idealized Model for Plasma Acceleration in an MHD Channel", AIAA Journal, Mar. 1983, Volume 21, Number 3

[9] J.L. Lawless and V.V. Subramaniam, "Theory of Onset in Magnetoplasmadynamic Thrusters", Journal of Propulsion and Power, Vol. 3, No. 2, Mar.-Apr. 1987

[10] M. Martinez-Sanchez, "The Structure of Self-Field Accelerated Plasma Flows", AIAA/DGLR/JSASS 19th International Electric Propulsion Conference, May 1987

[11] M. Mitchner and C. Kruger, *Partially Ionized Gases*, John Wiley and Sons, New York, 1973

[12] Scott Miller, SM Candidate, Dept. of Aeronautics and Astronautics, M.I.T., private communication

[13] H. Minakuchi and K. Kuriki, "Magnetoplasmadynamic Analysis of Plasma Acceleration", IEPC-84-06, AIAA/DGLR/JSASS 17th International Electric Propulsion Conference

[14] Won-Taek Park and Duk-in Choi, "Two-Dimensional Model of the Plasma Thruster", Journal of Propulsion and Power, Mar. - Apr. 1988, Volume 4, Number 2

[15] Patrick J. Roache, *Computational Fluid Dynamics*, Hermosa Publishers, Albuquerque NM

[16] V.V. Rusanov, "The Calculation of the Interaction of Non-Stationary Shock Waves and Obstacles", J. Computational Math and Mathematical Physics USSR, Number 2, 1962

[17] E.J. Sheppard, Doctoral Candidate, Dept. of Aeronautics and Astronautics, M.I.T., private communication

[18] P.C. Sleziona, Auweter-Kurtz, M. and H.O. Schrade," Numerical Codes for Cylindrical MPD Thrusters, 88-038, DGLR/AIAA/JSASS 20th International Electric Propulsion Conference", West Germany, Oct. 1988

[19] V.V. Subramaniam and J.L. Lawless, "Onset in Magnetoplasmadynamic Thrusters with Finite- Rate Ionization", Journal of Propulsion and Power, Vol. 4, No. 6